BEN-GURION UNIVERSITY OF THE NEGEV

THE FACULTY OF ENGINEERING SCIENCES

DEPARTMENT OF MECHANICAL ENGINEERING

Design and Modelling of a Minimally Actuated Serial Robot

THESIS SUBMITTED IN PARTIAL FULFILLMENT OF THE REQUIREMENTS FOR THE M.Sc. DEGREE

By: Yotam Ayalon

Supervised by: Dr. David Zarrouk

July 2020

July 2020

BEN-GURION UNIVERSITY OF THE NEGEV

THE FACULTY OF ENGINEERING SCIENCES

DEPARTMENT OF MECHANICAL ENGINEERING

Design and Modelling of a Minimally Actuated Serial Robot

THESIS SUBMITTED IN PARTIAL FULFILLMENT OF THE REQUIREMENTS FOR THE M.Sc. DEGREE

By: Yotam Ayalon

Supervised by: Dr. David Zarrouk

Author: Yotam Ayalon   Date: **19.07.2020**

Supervisor: David Zarrouk   Date: **19.07.2020**

Chairman of graduate studies committee: ד"ר בני בר-און
יו"ר לימודי מוסמכים
המחלקה להנדסת מכונות   Date: 21.7.20

July 2020

Abstract

In this project we present a minimally actuated overly redundant serial robot (MASR). The robot is composed of a planar arm comprised of ten passive rotational joints and a single mobile actuator that travels over the links to reach designated joints and rotate them. The joints remain locked, using a worm gear setup, after the mobile actuator moves to another link. A gripper is attached to the mobile actuator thus allowing it to transport objects along the links to decrease the actuation of the joints and the working time. A linear stepper motor is used to control the vertical motion of the robot in 3D space. Along the project, we present the mechanical design of the robot with 10 passive joints and the automatic actuation of the mobile actuator. We also present an optimization algorithm and simulations designed to minimize the working time and the travelled distance of the mobile actuator. Multiple experiments conducted using a robotic prototype depict the advantages of the MASR robot: its very low weight compared to similar robots, its high modularity and the ease of replacement of its parts since there is no wiring along the arm, as shown in the accompanying video.

Keywords: Serial robot, Minimal actuation, Mobile actuator, Mechanical design

Acknowledgments

First and foremost, I would like to express my sincere gratitude to my supervisor, Dr. David Zarrouk, for the continuous support of my thesis and research, for his patience, understanding, motivation, and most of all, for the knowledge he shared with me. It has been a great experience being part of the Bio-inspired Laboratory, which I am sure will continue to thrive and flourish under David's leadership for many years to come.

I would also like to express my very profound gratitude and appreciation to my parents, Yehuda and Levana Ayalon, for providing me with financial support throughout my years of study and for their unconditional love all through the years of my life. Finally, I must express my enormous gratitude for my beloved wife, Mrs. Noam Cohen, for constantly supporting me and for her thoughtfulness throughout my years of study. This accomplishment would not have been possible without them.

This research was supported in part by the Israel Ministry of Science and Technology and by the Pearlstone center for Aeronautical Studies.

Table of Contents

Nomenclature

Symbol	Units	Meaning
A	mm^2	The cross-section area
A_b^a	-	Homogeneous transformation matric from coordinate system b to coordinate system a
d_{LINK}	mm	The distance from the line (collinear) along the link j
d_T	mm	The distance travelled by the mobile actuator
Δd	mm	The distance from the target (error)
E	GPa	Young's modulus
f_{TIP}	mm	The proximity function
f_{OR}	deg	The orientation function
f_{STOPS}	-	The weight of the number of actuated joints
f_{JOINTS}	mm	The function of the distance between the joint to the target
$F()$	-	Cost function
F_{links}	N	Force due to the links' weight
F_{act}	N	Force due to the mobile actuator's weight
F_{y_A}	N	The vertical force at the fixed edge
$i_{rot\text{-}sys}$	-	The rotation mechanism transmission
I_y	m^4	Moment of inertia of the cross-section
J_j	-	Jacobian matrix
L	mm	Length of each link
M_A	Nm	The bending moment at the fixed edge
$M_I(x)$	Nm	The internal moment of the cross-section in section I
$M_{II}(x)$	Nm	The internal moment of the cross-section in section II
n	-	Number of links including the base link
N	-	Number of links and joints
$\overline{r}_j^{(a)}$	-	Vector from coordinate system a to joint j
Rot_{z,θ_a}	-	Rotation matric of coordinate system a
T_{stop}	sec	Time required to start and stop the mobile actuator
ΔT	sec	Time to reach the target
$Trans_{x,L}$	-	Translation matric along x axis
V_z	m/sec	Lifting and lowering velocity
V_m	m/sec	Translating velocity of the mobile actuator
Xi	-	Arm's initial position and orientation

Xf	-	Arm's final position and orientation
X_j	-	Position and orientation of joint *j*
$\dot{X}_j$	-	Velocity of joint *j*
$\bar{x}_{COM}$	mm	The distance from the fixed edge to centre of mass
x_{Edge}	mm	The distance from the fixed edge to the free edge
$y_I(x)$	mm	The beam's deflection in section I
$y_{II}(x)$	mm	The beam's deflection in section II
$Z_{partial\text{-}gear}$	-	Number of teeth of the partial gear
$Z_{link\text{-}gear}$	-	Number of teeth of the spur gear at the both sides of the links
Z_{worm}	-	Number of teeth of the worm module
$Z_{worm\text{-}gear}$	-	Number of teeth of the printed worm gear
α_j	deg	Orientation of link *j* in the word coordinate system (no.0)
ε	-	The strain
θi	deg	Arm's initial configuration
θ_j	deg	The relative angle of joint *j*
$\theta_{resolution}$	deg	The resolution of the angle displacement
Δθ	deg	The angle's error of the end-effector from the target
$\Delta\theta_j$	deg	The rotation of joint *j*
σ	Pa	The stress
ω	deg/sec	The rotation mechanism velocity

List of Figures

List of Tables

1. Introduction

Conventional serial robots are composed of several rigid links connected to each other using actuated joints. Most 3-dimensional commercially available serial robots have between 4 and 7 degrees of freedom. In tasks that call for maneuvering in confined spaces, traditional serial robots are often insufficient. In some industries the inability to do certain tasks because of restricted access has major commercial significance.

The prime reason for developing hyper redundant robots (alternatively known as snake robots), is their ability to navigate around obstacles and in highly confined spaces. They are typically actuated using 10 to 20 motors. Extensive research over the past several decades has generated many different configurations and mechanisms for a variety of applications such as search and rescue operations, as well as maintenance and medical applications for minimally invasive procedures. Due to their relatively low weight, these robots are possible candidates for planetary exploration and space satellite maintenance.

Control and motion planning with serial robots nevertheless present formidable challenges in terms of high dimensionality analysis. Numerous researchers have addressed the planning problem using different optimization strategies that have led to substantial advances.

To simplify the kinematics and actuation, and minimize the dynamic modeling, we suggested in previous works a minimally actuated reconfigurable track robot [32], and a preliminary design concept serial robot with a mobile actuator [33].

Figure 1.1. The minimally actuated serial robot MASR is a newly developed robot with a large number of joints and a single mobile actuator. The mobile actuator travels along the links to actuate the joints.

Here we extend on these works [32][33], and present a Minimally Actuated Serial Robot (MASR) that incorporates multiple characteristics and advantages from both minimally actuated robots and hyper redundant robots. The MASR is a serial robot consisting of multiple links connected through passive joints and one or more mobile actuator(s). The MASR's uniqueness is that the moveable actuators translate over the links to reach a given passive joint and adjust it to the desired angular orientation. The joint passively preserves its angular orientation until it is actuated again. By implementing this design which decouples the links from the motors, the MASR robot can be easily reshaped to the intended task by adding or removing links or by replacing the moveable actuators. The smaller number of motors and the simplicity of the design allow for increased reliability, smaller weight, lower costs and high modularity.

This project is organized as follows; A short background for better understanding the importance of using hyper-redundant robots, especially at the space exploration field, is presented in Section 2. Section 3 deals with the design of the robot, including the robot's structure and materials used for manufacturing. The actuation and control of the robot are presented in Section 4. In section 5 we perform several analyses, including the kinematic and dynamic, and the structural rigidity. Section 6 and 7 focus on the motion planning algorithm of the robot and the experiments we have performed.

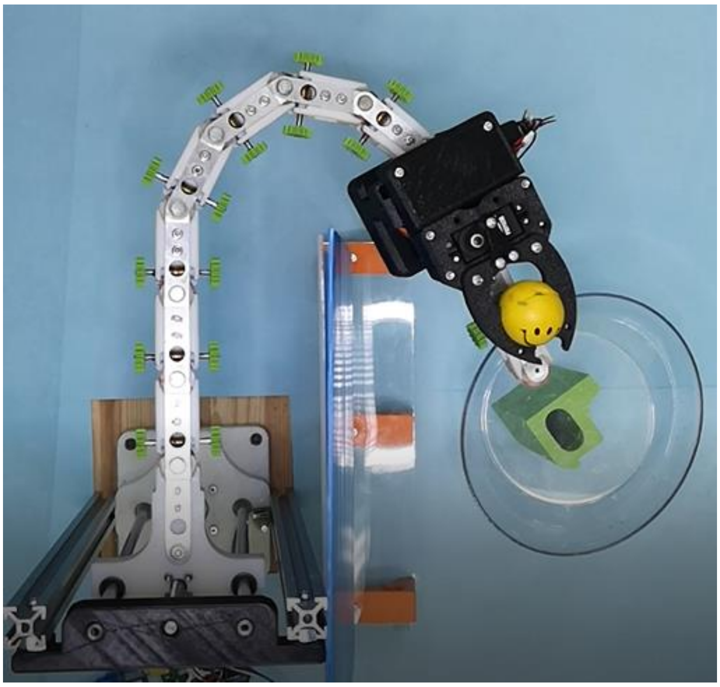

Figure1.2. The minimally actuated serial robot MASR from a top view while carrying an object to the target.

2. Background

This section reviews some theoretical background relevant for this research, including a brief review about the importance of using serial robots in the space exploration field and about the development of hyper-redundant robots over the last several decades.

2.1 Space Exploration

With rapid technological advancement over the past decades, it is evident that there is a significant growing need to combine robots in space exploration missions [3] [4]. In order to perform future space explorations over the long-term by reducing human explorers' workload, mission costs, fatigue-driven errors and risks, robots will have to be an integral part of missions' design.

Spacewalk outside the space station or extravehicular activities are considered to be one of the riskiest activities for astronauts, due to limited time humans can spend in a fragile, pressurized spacesuit, exposed to a huge amount of radiation. Serial robots can be used to complete mundane and unsafe tasks for astronauts, such as moving space assets from one point to another, performing daily maintenance tasks outside the spacecraft etc., while freeing up time for the astronauts to do their critical tasks.

Figure 2.1. Astronaut Stephan K. Robinson anchored to the end of Canadarm 2 during STS-114, 2005.

Space robotic arms, such as Canadarm2, the Canadian space shuttle robotic arm [5], the American express rail arm [6], and the ETS-VII arm [7], are used to replace or assist human astronauts in the implementation of on-orbit transportation or assembly, to repair satellites, to prolong the life of the spacecraft through the operations like capturing space facilities, repairing and maintaining, releasing and recovering [8].

One of the biggest challenges in space missions is the spacecraft weight. Every pound that is carried to space, required fuel to do so. The more the vehicle weight, the fewer passengers and payload the vehicle can carry. Space exploration mission usually takes several months or years, and there is a large variety of tasks to be done during the mission. Thus, the ability to adjust an individual robot to perform different tasks with different properties, is highly necessary.

Figure 2.2. An illustration of one of the possible application MASR can be used for.

2.2 Serial Robots

Serial robots are made up of several links connected by actuated joints. The number of degrees of freedom (DOF) of a serial robot depends on the number of links and joints and the types of joints used for the construction of the mechanism. In order to manipulate an object freely in the tree-dimensional space, a serial robot should possess 6 degrees of freedom. Serial robot is considered as a general-purpose robot if it indeed possesses 6 DOF, a redundant robot if it possesses more than 6 DOF, and a deficient robot if it possesses less than 6 DOF [9]. A redundant robot provides more freedom to move around obstacles and operate in a tightly confined workspace. The workspace of a manipulator is defined as the volume of space the end-effector can reach. Two different definitions of workspace are frequently used: *reachable* and *dextrous* workspace. A reachable workspace is the volume of space within which every point can be reached by the end-effector in at least one orientation. A Dextrous workspace is the volume of space within which every point can be reached by the end-effector in all possible orientations.

Serial robots offer multiple advantages as they are accurate, quick to react and provide a large work volume. They are used and integrated in the industry in many applications, generally for tasks that require repeatability such as pick-and-place, painting and welding operations, with many companies offering multiple off-the-shelf prototypes [10][11]. However, the main setback of the serial robots is their force to weight ratio and their inability to operate in confined spaces and through obstacles. To overcome this challenge, snake robots which are practically serial robots made of large number of joints, about 20 or more, were part of an extensive research over the past several decades [12][13].

2.3 Hyper-Redundant Robots

Hyper-redundant robots are considered to be as part of the robotic snake family. These robots are composed from serially connected links and characterized by possessing a large kinematic redundancy. These manipulators can be analogous in morphology and operation to snakes, elephant trunks or tentacles [14]. Because of their highly articulated structures, these robots are well suited for operation in highly constrained environments. It is an evident that these robots are the subject of extensive research over the past several decades with many different configurations, mechanisms, control strategies, and motion planning algorithms [15]-[19]. To our knowledge, the earliest hyper-redundant robot design is date to the late 1960's [20]. Numerous other authors have suggested hyper-redundant designs or developed hyper-redundant robot mechanisms. These robots are mainly used in application such as search and rescue operations [21]-[29], medical applications for minimally invasive procedures [30]-[35], and for planetary exploration and space satellite maintenance [36]-[39].

Hyper-redundant robots indeed present a great potential for different applications in confined spaces, pipes and rubbles. However, there are some serious challenges facing these robots. In order to achieve a good performance with highly accuracy of the end-effector, a significant portion of these robots are designed to maximize the stiffness of their manipulator by using heavy materials, creating a bulky design. Adding the fact that most of them are using a large number of actuators, these robots are considered to be inefficient in terms of power consumption with respect to the allowable operational payload [40].

In addition to the mechanical drawbacks, the hyper-redundant robots also accompanied by a formidable challenge while trying to create algorithms for planning their motions. Most of the standard methods developed for robot motion planning

[41][42] are not suitable for planning the motion of the hyper-redundant robots due to their high-dimensional coordinate space. Gregory Chirkjian was among the first to propose suitable motion planning algorithms for hyper-redundant robots at the beginnings of the 90th [43]-[46]. Yet, in his works, Gregory made several approximations, such as the robotic snake was considered as a continuous modal function and the obstacles expressed as boundary constraints on the robot's shape. Following Gregory's works, many recent algorithms have addressed obstacle avoidance schemes for hyper-redundant robots [47]-[54]. However, these motion planning algorithms are usually time consuming and not always implementable in real-time applications.

In order to overcome the mentioned shortcomings and to improve industrial productivity while still achieving high redundancy, flexible robots have been proposed as an alternative [55][56]. Also known as continuum robots, these flexible robots which consist of a flexible continuous structure, are considered as an infinite number of degrees-of-freedom mechanism, and are inspired by several biologic applications, such as snakes, elephant trunks, lizard tongues and octopus' arms. The advantages of flexible robots over hyper-redundant robots are the followings; their weight is significantly lower than their opponents, they can produce higher operational speed, and in some cases, they consist smaller number of actuators. Yet, developing models that accurately simulate the motion of these robots are highly required, since it might be a complex Multiphysics problem that can involve simultaneous analysis of several fields, such as solid and fluid mechanics, kinematics, chemical kinematics, etc. Moreover, achieving progress with new approaches of path planning that are computationally efficient, is critical to make a real-time path-planning viable. These drawbacks leave them, as of today, unsuitable for tasks that require relatively high degree of accuracy.

We can clearly notice that there are several challenges that characterized both: the hyper-redundant and the continuum robots. These challenges include minimizing the robot's weight while still achieving robust mechanism, minimizing the number of actuators for efficient power consumption and developing a time efficient motion planning algorithm that will be real-time viable.

Saying all that, developing a novel hyper-redundant robot, which characterized by low weight and size, high modularity performance, and by small number of actuators, will enable to execute different tasks over outstanding advantages, especially in the space exploration field.

3. Mechanical Design

This section reviews the mechanical design of the robot and its main parameters, as well as the materials used for the robot and the design specification.

The MASR robot presented in this project (Figure 3) is composed of a serial planar arm with 10 joints, a linear actuator that can displace the arm in the vertical direction and a mobile actuator that can travel along the links and rotate the joints when needed. Considerable effort was invested in keeping the design of the robot as simple as possible and reducing its weight.

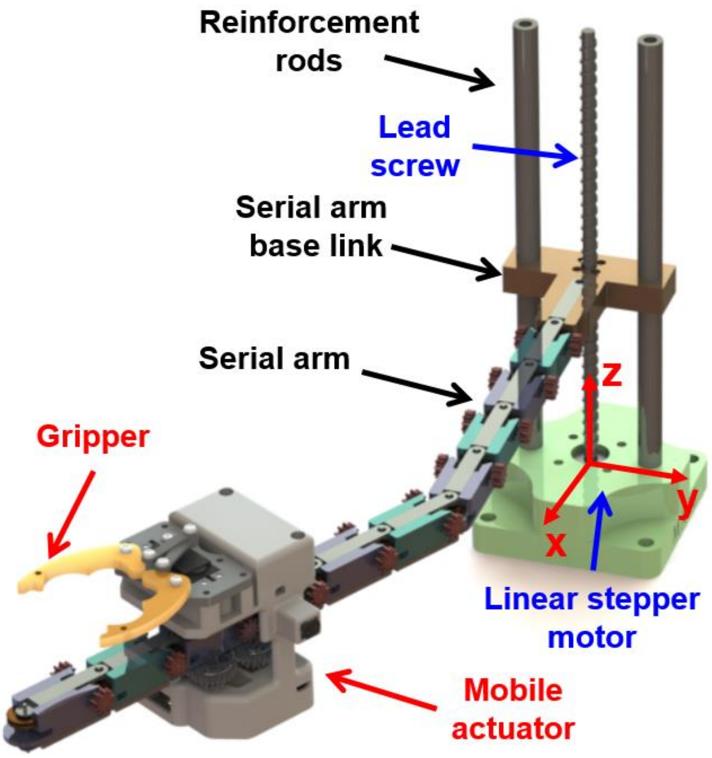

Figure 3.1. The mechanical design of MASR robot. The robot consists of a planar serial arm with 10 passive joints actuated by a mobile actuator. The mobile actuator that can travel over the links is fitted with a gripper to carry objects along its path. The vertical motion is actuated by a linear stepper motor.

3.1 Product Design Specifications

The MASR robot presented in this paper is an improvement of the last version of the robot, developed by Lior Damti and Dr. David Zarrouk. The current version was designed in order to achieve a fully working prototype, which will be mechanically stronger than the previous version, will enable to execute missions in 3-Dimensional workspace, and will be operated automatically via a controller. The new design requirements were formed in order to overcome the following shortcomings of the previous version:

- The robot's operation capabilities were limited to the 2-Dimensional workspace, meaning it could execute tasks only in the horizontal plane.
- The previous prototype had a significant deflection along the robot's mechanism.
- The actuator struggled to translate over the links, especially while the relative angle was grater that $25°$. The main cause was due to an insufficient grip between the actuator's wheels and the serial arm.
- The operation of the previous prototype was enabled only by a remote control and had any automatically abilities.

Yet, we must consider some aiming characteristics in our design, as follows:

- The robot must be lightweight, yet stiff enough to sustain his own weight and external forces.
- The links must be easily connected to each other in order to enable the robot high modularity performance.
- The mobile actuator must be smoothly shifted from one point to another, without changing the relative angles of the joints.

- The manufacturing costs must be lowest as possible, while achieving similar mobility (albeit slower) to the typical hyper-redundant robot.

3.2 Robot's Structure and Components

This chapter reviews the general structure of MASR robot to better understand its operation. The MASR structure can be described via three main assemblies. The first one is the serial arm, the second assembly is the mobile actuator and the third one is the vertical driving mechanism.

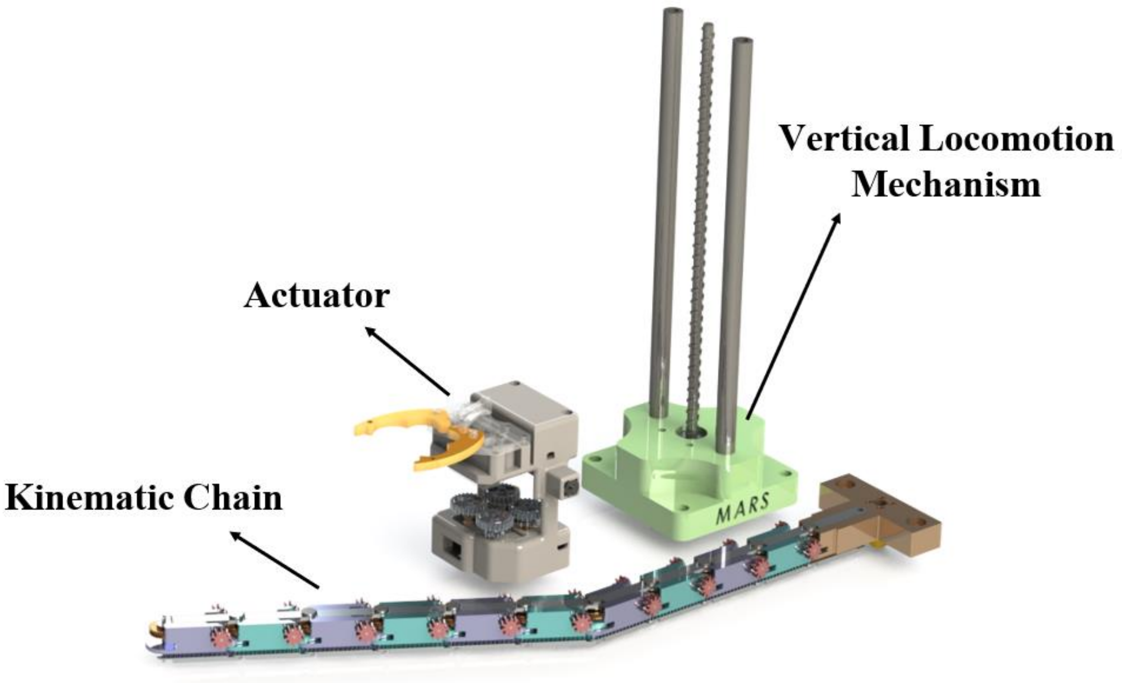

Figure 3.2. The MASR robot main assemblies. There are 3 general assemblies: the serial arm, the mobile actuator and the vertical driving mechanism.

3.2.1 The Serial Arm

The serial arm of the current design is composed of 10 identical links (Figure 4). The links are 5 cm long and 2 cm wide and are attached to each other through rotational joints. The length of the arm fitted with 10 links is 50 cm and its weight is 0.35 kg. A worm gear transmission is used to rotate the joints at a ratio of 1:38. The worm gear ensures that the links remain locked at the desired angle after the actuation is completed. The relative angle θ_j between two adjacent links (j-1 and j) can be varied in the range of [-45º, 45º].

At their bottom, the links have a gear rack designed to increase the traction of the mobile actuator when traveling over the links and to eliminate the possibility of sliding. In order to increase the rigidity of the 3D printed (plastic) links, aluminum supporting rods were added at their top and bottom. The weight of each link including the aluminum support is 30 grams. Magnets were attached at the center of the joints to help the mobile actuator identify its location while travelling along the arm.

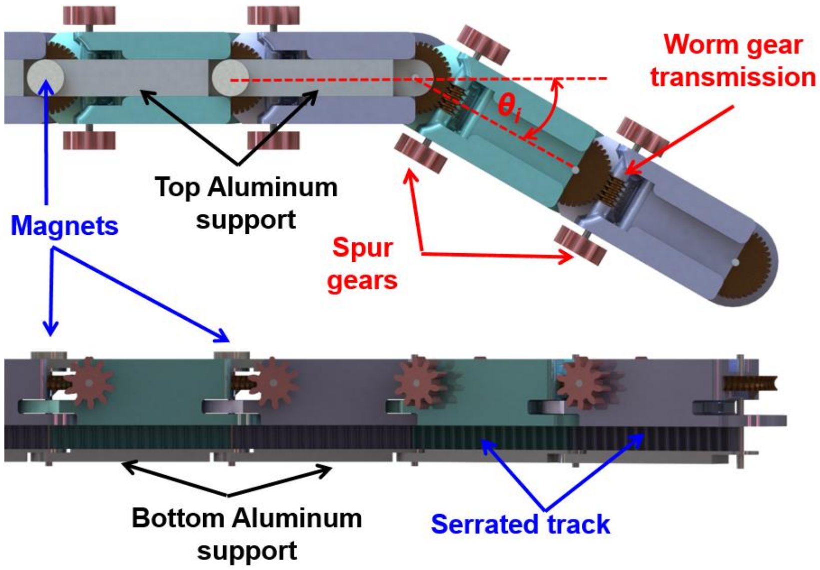

Figure 3.3. The robotic arm is composed of 10 links attached through rotational joints. A worm gear transmission is used to actuate the links and ensure that the relative angle is preserved when the mobile actuator departs from the joint.

3.2.2 The Mobile Actuator

The mobile actuator, presented in (Figure 5), is designed to travel over the links, stop at a designated location to rotate the joints and grasp objects using the gripper. It is composed of three separate mechanisms: the locomotive, the joint rotation mechanism and the gripper.

a) The Locomotive

The locomotive carries the actuator along the links using four serrated wheels. Two of the wheels on the one side are actuated using a rotational motor and the other two wheels, located on the other side, are passively actuated. To enable the locomotive to travel over curved joints (up to 45 degrees), the axes of the passive wheels are fixed on a rotational joint. This joint is fitted with springs, allowing the wheels to conform to the variation in the track and apply a gripping force on the tracks of the links

b) The Joint Rotation Mechanism

The mobile actuator is fitted with a spur gear with partial gearing. When the mobile actuator reaches a specific link j, it engages the spur gear of the joint/link and rotates it. As a result, the relative angle between the two adjacent links (j and j-1) is changed (see Figure 5 and video). The partial gearing (four teeth per revolution) of the rotation mechanism is used to avoid unwanted collisions between the spur gear of the locomotive and links as the mobile actuator travels along the arm. The worm gear assembly has a ratio of 1:38, and the spur gear's ratio is 1:3, so that each full revolution of the partial spur gear will result in a 3.2 degrees rotation of the joint (see Appendix A).

c) The Gripper

The gripper, attached to the mobile actuator, is an off-the-shelf two-finger mechanism actuated by a servo motor. It can hold objects at widths of 2.5 cm to 10.5 cm. Note that in this robot, the gripper is not fixed to the last link of the robot but rather to the mobile actuator. As a result, the mobile actuator can travel over the links to grasp objects and translate them along the arm. More sophisticated grippers with more fingers can be attached to the mobile actuator if needed. The gripper can also be replaced with a welding tool, a saw, or a paint brush for example, depending on the application requirements.

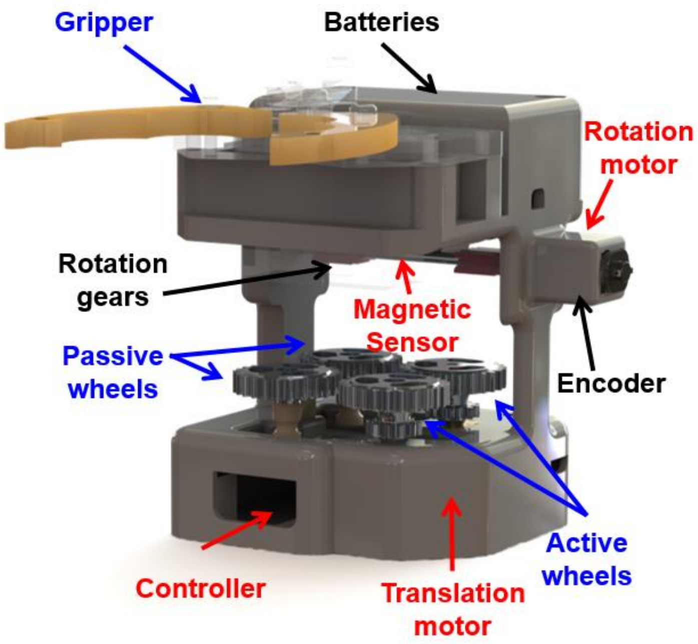

Figure 3.4. The mobile actuator is composed of a locomotive mechanism, a rotation mechanism and a gripper. The mobile actuator holds its controller and batteries onboard.

3.2.3 The Vertical Locomotion Mechanism

Vertical motion (z direction) is enabled by a lead screw rotated with a stepper motor located at the base of the robot. The diameter of the screw is 8 mm and its pitch 8 mm. Because the stepper motor makes 200 steps per revolution, the nominal accuracy of the motion is 0.04 mm. To reinforce the structure to prevent bending, two 10 mm steel rods are attached to the base of the robot (Figure 3). The total range of the vertical motion is 38 cm.

3.3 Manufacturing

The robot is mostly manufactured from 3D printed materials. The links, which require high resolution, were printed using a Polyjet printer (Object Connex 350) and the mobile actuator was printed using an FDM printer. To increase the strength of the serial arm and minimize bending, 3 mm thick aluminum rods were attached on the top and bottom of the links. Since there is no wiring along the links, their replacement is very simple.

4. Robot's Actuation and Control

This section reviews the actuation of the robot and the components we used to design the control loop.

4.1 Actuation

The MASR robot, including its gripper, is actuated using a total amount of four motors:

- One 12 V stepper motor to move the arm in the vertical direction. The stepper motor produces a torque of 36 Ncm. For the given lead screw diameter and pitch (both 8 mm) and assuming that the coefficient of friction is 0.3, the motor and lead screw setup can produce an estimated vertical force of 140 N [31].
- Two DC motors: one motor to drive the mobile actuator along the links, and the other motor to rotate the joints of the links. Both motors are 12 mm in diameter (6-9 Volts manufactured by Pololu), which can be purchased at different gear ratios and can be fitted with magnetic encoders.
- An off-the shelf servo motor to actuate the gripper.

4.2 Control

The robot is controlled by two electronic control boards that are synchronized using RF module communication. The mobile actuator is controlled with a Teensy 3.5 controller (compatible with Arduino software) that controls its locomotion, its rotational mechanism and its gripper. The angular displacement of the rotational mechanism is measured using a magnetic encoder fitted to the motor's shaft and yields 12 counts per motor revolution. The motors are powered by two 3.7 Volts 800 mAh LiPo batteries connected in series.

To ensure that the mobile actuator stops accurately at the precise location to engage the gears of the links and rotate the joints, tiny magnets were inserted in the centers of the joints and a magnetic Hall effect sensor (A1302) was attached to the mobile actuator. The stepper motor that actuates the vertical motion is controlled with an Arduino Uno board. The two controllers communicate via a NRF24L01 Radio Transceiver Module that transmits and receives commands and other data such as location and orientation between the two controllers.

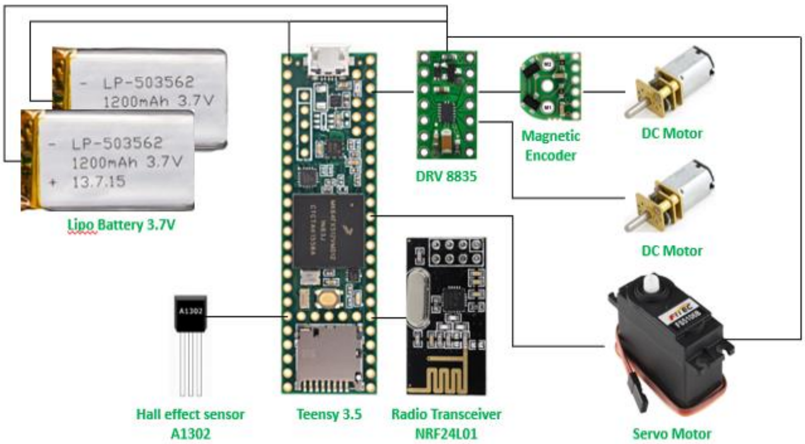

Figure 4.1. Wiring scheme of the mobile actuator’s control loop.

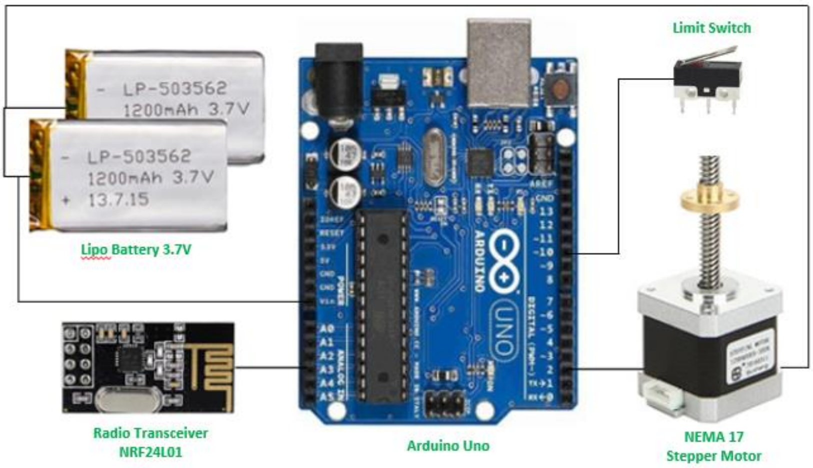

Figure 4.2. Wiring scheme of the vertical locomotion’s control loop.

4.3 Sequence of Operation (SOO)

This section describes the SOO of the manipulator. It should be noted that we have created two separate programs in Arduino® software, one for the Teensy microcontroller and the second for the Arduino microcontroller. The SOO is as follows:

a) The operator should insert the following details into the Teensy's program: the desired joints and the relative angles, the height of the manipulator and the gripper's state at every single step during the program.

b) During the robot's operation, The Teensy always sends the requested height to the Arduino, while the last sends commands to the stepper motor to drive the robot to the desired height.

c) The mobile actuator translates along the serial arm. Once it reaches a desired joint, the mobile actuator stops, and the rotation motor starts rotating while changing the relative angle. The encoder sends to the Teensy the number of revolutions has been counted, and the Teensy calculates the angle's displacement by a simple conversion, using the transmissions ratio.

d) The gripper changes its state as defined.

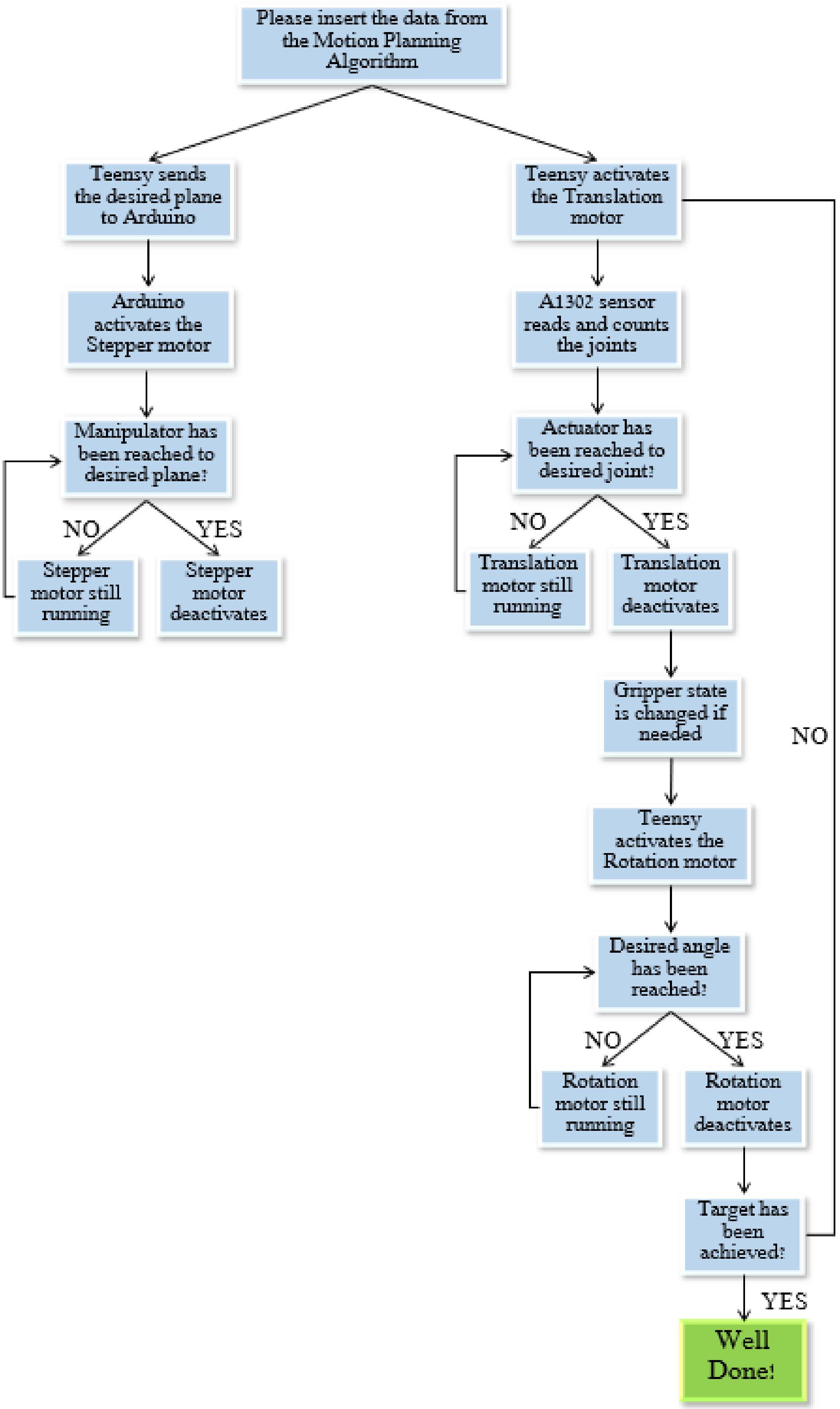

Figure 4.3. Sequence of Operation of the control loop.

5. Kinematic Model

This section reviews the kinematic model of the robot, including the position and speed, and the workspace of the manipulator.

5.1 Position and Speed

A configuration of a manipulator is a complete specification of the location of every point on the manipulator. The set of all possible configurations is called the configuration space. In our case, if we know the values of the relative angles, then it is straightforward to infer the position of any point along the manipulator, since the individual links of the manipulator are assumed to be rigid, and the base of the manipulator is assumed to be fixed. In order to receive a general configuration analysis, we assume that our robot is composed of N identical links (not including the base link) whose length is L, connected using N rotational joints. Since the manipulator is confined to the horizontal plane (x,y) and the linear screw to the vertical direction (z), the motion of the two mechanisms can be decoupled and the analysis can be performed separately. The links are numbered from 0 (the base link) to N which represents the last link in the serial arm. The joint angle j between the links j-1 and j is denoted by θ_j, and the relative orientation of link j to the base link by α_j.

In order to find a general equation, describing the location of every single joint along the kinematic chain, we first examined the simplest case while the kinematic chain consists from only two equal joints (see Fig. 5.1). in order to find the locations of the joints in the world coordinate system, we used the DH convention to form the homogenous transformation matrices.

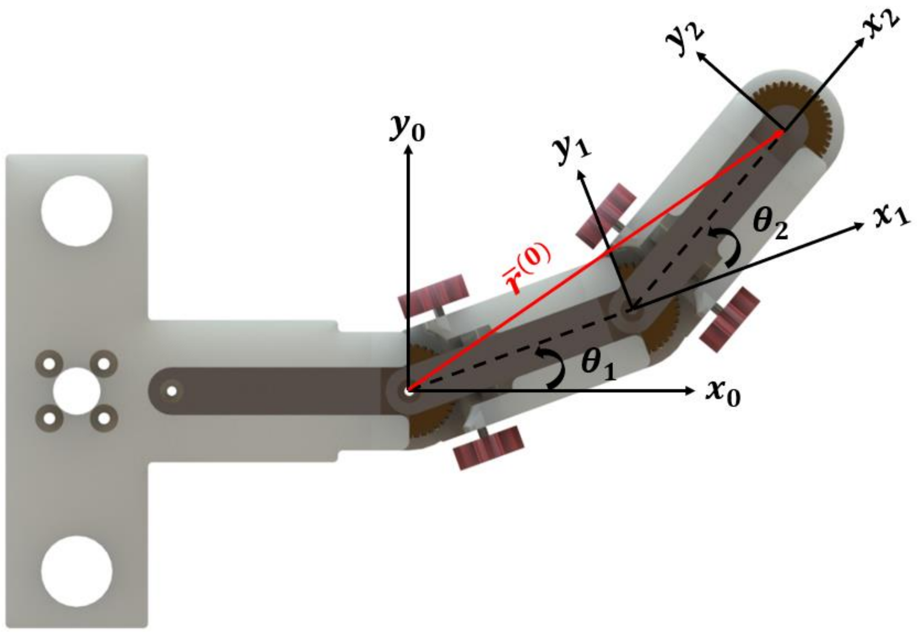

Figure 5.1. Two equal links connected to the base link and experiencing a rotation around *z* axis.

The homogeneous transformation matric of A_1^0 (the origin of coordinate system no.1 presented in the world coordinate system) would be:

$$A_1^0 = Rot_{z,\theta_1} \cdot Trans_{x,L} = \begin{bmatrix} \cos\theta_1 & -\sin\theta_1 & 0 & 0 \\ \sin\theta_1 & \cos\theta_1 & 0 & 0 \\ 0 & 0 & 1 & 0 \\ 0 & 0 & 0 & 1 \end{bmatrix} \begin{bmatrix} 1 & 0 & 0 & L \\ 0 & 1 & 0 & 0 \\ 0 & 0 & 1 & 0 \\ 0 & 0 & 0 & 1 \end{bmatrix} \tag{1}$$

$$A_1^0 = \begin{bmatrix} \cos\theta_1 & -\sin\theta_1 & 0 & L\cos\theta_1 \\ \sin\theta_1 & \cos\theta_1 & 0 & L\sin\theta_1 \\ 0 & 0 & 1 & 0 \\ 0 & 0 & 0 & 1 \end{bmatrix} \tag{2}$$

Where Rot_{z,θ_1} and $Trans_{x,L}$ are the rotation and translation matrices of coordinate system no.1, respectively.

The homogeneous transformation matric of A_2^1 (the origin of coordinate system no.2 presented in coordinate system no.1) would be:

$$A_2^1 = Rot_{z,\theta_2} \cdot Trans_{x,L} = \begin{bmatrix} \cos\theta_2 & -\sin\theta_2 & 0 & 0 \\ \sin\theta_2 & \cos\theta_2 & 0 & 0 \\ 0 & 0 & 1 & 0 \\ 0 & 0 & 0 & 1 \end{bmatrix} \begin{bmatrix} 1 & 0 & 0 & L \\ 0 & 1 & 0 & 0 \\ 0 & 0 & 1 & 0 \\ 0 & 0 & 0 & 1 \end{bmatrix} \tag{3}$$

$$A_2^1 = \begin{bmatrix} \cos\theta_2 & -\sin\theta_2 & 0 & L\cos\theta_2 \\ \sin\theta_2 & \cos\theta_2 & 0 & L\sin\theta_2 \\ 0 & 0 & 1 & 0 \\ 0 & 0 & 0 & 1 \end{bmatrix} \tag{4}$$

The homogeneous transformation matric of A_2^0 would be:

$$A_2^0 = A_1^0 \cdot A_2^1 = \begin{bmatrix} \cos(\theta_1+\theta_2) & -\sin(\theta_1+\theta_2) & 0 & L\cos\theta_1 + L\cos(\theta_1+\theta_2) \\ \sin(\theta_1+\theta_2) & \cos(\theta_1+\theta_2) & 0 & L\sin\theta_1 + L\sin(\theta_1+\theta_2) \\ 0 & 0 & 1 & 0 \\ 0 & 0 & 0 & 1 \end{bmatrix} \tag{5}$$

In order to find the location joint no.2, expressed in the world coordinate system, we will use the following connection:

$$\begin{bmatrix} \bar{r}_2^{(0)} \\ 1 \end{bmatrix} = A_2^0 \cdot \bar{r}_2^{(2)} \tag{6}$$

Where $\bar{r}_2^{(0)}$ is the vector from the world coordinate's origin to joint no.2, and $\bar{r}_2^{(2)}$ is the vector from the origin of coordinate system no.2 to joint no.2. Since joint no.2 is located exactly at the origin of coordinate system no.2, $\bar{r}_2^{(2)}$ would be:

$$\bar{r}_2^{(2)} = [0\ \ 0\ \ 0\ \ 0]^T \tag{7}$$

Saying all that, the location of joint no.2, expressed in the world coordinate system, would be:

$$\begin{bmatrix} x_0 \\ y_0 \\ z_0 \\ 1 \end{bmatrix}_{Edge\_no.2} = \begin{bmatrix} L\cos\theta_1 + L\cos(\theta_1+\theta_2) \\ L\sin\theta_1 + L\sin(\theta_1+\theta_2) \\ z_2 \\ 1 \end{bmatrix} \tag{8}$$

At the same manner, we can say that the location of the edge of link no.1, expressed in the world coordinate system, is:

$$\begin{bmatrix} x_0 \\ y_0 \\ z_0 \\ 1 \end{bmatrix}_{Edge\_no.1} = \begin{bmatrix} L\cos\theta_1 \\ L\sin\theta_1 \\ z_1 \\ 1 \end{bmatrix} \tag{9}$$

Therefore, the position of joint j (x_j, y_j, z) of the robot and its orientation α_j are given by:

$$\mathbf{X_j} = \begin{bmatrix} x_j \\ y_j \\ z \\ \alpha_j \end{bmatrix} = \begin{bmatrix} L\sum_{m=1}^{j}\cos\left(\sum_{m=1}^{n}\theta_m\right) \\ L\sum_{n=1}^{j}\sin\left(\sum_{m=1}^{n}\theta_m\right) \\ z_j \\ \sum_{m=1}^{j}\theta_m \end{bmatrix} \tag{10}$$

The mobile actuator in our robot can either travel along the links or rotate the joints. Therefore, the speed $\dot{X}_j$ of a joint j can be calculated using the Jacobian matrix J_j like other regular serial robots:

$$\dot{\mathbf{X}}_{\mathbf{j}} = \mathbf{J_j}\begin{bmatrix} \dot{\theta}_1 \\ \vdots \\ \dot{\theta}_j \\ \dot{z} \end{bmatrix} \tag{11}$$

where the Jacobian matrix is defined as:

$$\mathbf{J_j} = \left[\frac{\partial X}{\partial \theta_1} \cdots \frac{\partial X}{\partial \theta_j}, \frac{\partial X}{\partial z}\right] \tag{12}$$

Note that since a single mobile actuator is currently being used, the different joints of the serial arm can be actuated one at a time. The total time required to reconfigure the angles of the joints and reach a specific target is composed of the time required to travel along the links, to engage the joints, rotate them and disengage from them. The vertical motion along the vertical direction can be performed in parallel to the motion of the serial arm.

If we assume a constant lifting and lowering velocity V_z of the vertical motor and constant linear and rotational speeds of the mobile actuator, respectively V_m and ω, the time required to reach a target is:

$$\Delta T = Max \begin{cases} \frac{1}{\omega}\sum_{1}^{N}\left|\Delta\theta_j\right| + \frac{d_T}{V_m} + n \cdot T_{stop} \\ \frac{\Delta z}{V_z} \end{cases} \tag{13}$$

where $\Delta\theta_j$ is the rotation of joint j, d_T is the total distance travelled by the mobile actuator, n is the number of rotated joints and T_{stop} is the time required to start and stop the mobile actuator.

5.2 The Workspace

Given that the joints in the current design are limited to rotating by a maximum of 45 degrees to either side, we determined the work volume of the serial arm in the 2D space as a function of the number of links. The work volume was determined by exhaustively searching the total space for possible solutions (not including orientation), using the motion planning algorithm presented in Section 6. At six links, the arm can already reach areas behind its base. The size of the work area (2D space) continues to increase with the number of links. The size of the workspace is nearly four times larger with 10 links compared to its size with 6 links. The size of the workspace as a function of the links is presented in 0

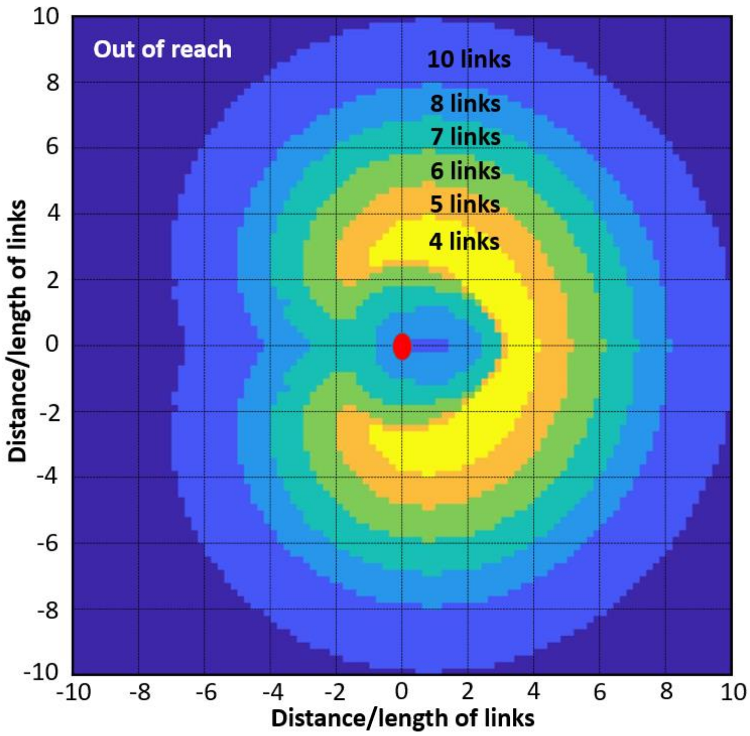

Figure 5.2. Top view of the work volume of the robot as a function of the number of links.

Table 5.1: Size of the workspace as a function of *N*.

No. of links N	4	5	6	7	8	10
Workspace [L^2]	8.3	18.9	35.8	58.7	83.5	136.7

6. 2D Motion Planning Algorithm

The MASR robot is a minimally actuated overly redundant robot, i.e., there is an infinite number of solutions to reach a specific point in the plane using the robotic arm. Our aim in this planning algorithm is to reduce the location error, the travelling distance of the mobile actuator, its number of stops to rotate the joints and the total time required to perform a task. Assuming an obstacle-free space, and that the arm's initial configuration is **θi**, (initial position and orientation **Xi**=(x_i,y_i,α_i)), the goal is to determine the joint rotation $\Delta\boldsymbol{\theta}_{\mathbf{j}}$ which will lead the arm to the final location **Xf**=(x_f,y_f,α_f).

Our algorithm is based on minimizing a cost function F(**Δθj**, **θi**, **Xf**) which combines the original orientation of the links, the proximity of the robot to the target point and the variation of the joint angles from the original to the final configuration. We minimized the function using Matlab's fmincon function which can find a local minimum within given upper and lower bounds (such as the minimum and maximum values of the rotation angle, negative 45 degrees to positive 45 degrees). To increase its chances of finding the global minimum and improve the results, we ran the function 100 times with different randomly chosen original solution guesses and the solution with the lowest cost function was chosen. Throughout this analysis, we assumed that the robot was composed of 10 identical links whose length *L* is 5 cm (similar to the experimental robot). In the following examples, solutions were accepted only if the maximum distance from the target was less than 0.2 cm and the orientation error of the last link was less than 0.5 degrees.

6.1 Reaching a Target with the Tip of the Last Link (LL)

Although the mobile actuator carries the gripper, in many applications grasping an object may be possible only if the gripper is located on the last link of the serial arm. In this case, the tip of the robot must reach the desired location and the last link must have the same orientation as the target. The cost function F is composed of the three functions, f_{TIP} and f_{OR} which respectively weigh the distance and orientation of the last link from the target and the function f_{STOPS} which weighs the number of the actuated joints.

$$F\left(\mathbf{\Delta\theta_j},\mathbf{\theta_i},\mathbf{X_f}\right) = f_{TIP} + f_{OR} + f_{STOPS} \tag{14}$$

The proximity function f_{TIP} is simply defined as the norm of the vector error of the tip of the robot from the target point:

$$f_{TIP} = norm\left(\mathbf{X_F} - \mathbf{X_N}\right) \tag{15}$$

The orientation function f_{OR} is the square of the difference between the orientation of the last joint to the orientation of the tip of the robot:

$$f_{OR} = 200\left(\alpha_N - \alpha_T\right)^2 \tag{16}$$

Its value was multiplied by 200 to increase its weight. The function's value becomes unity (equal to one) if the error is nearly 0.2 degrees (0.0035 Radians).

The function f_{STOPS} is negative and sums the values of the changes in the joints at the power n.

$$f_{STOPS} = -\sum_{j=1}^{N}\left|\Delta\theta_j^n\right| \tag{17}$$

If the power n is larger than 1, the algorithm attempts to increase the variation of the joints. Given that the sum of the variation is limited by the orientation of the last link, the algorithm attempts to reduce the number of active joints and increase their rotation.

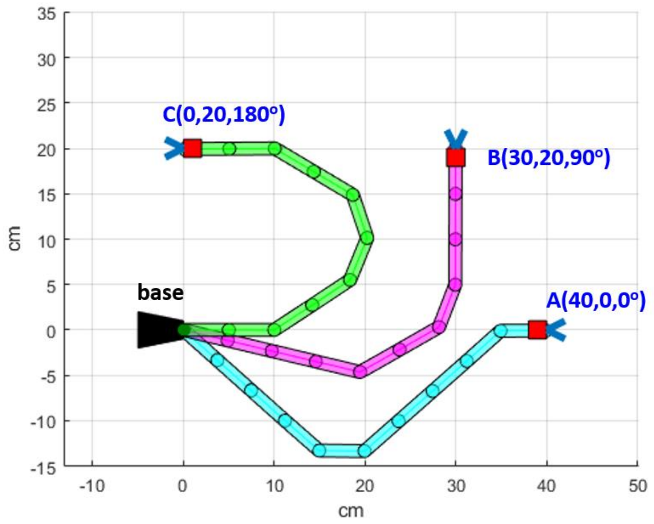

Figure 6.1. Starting from an initial configuration where all the joints were at 0 degrees, the robot reaches points A, B, and C using the LL method.

Table 6.1: Solution for A, B, and C using the "LL" Method.

Joint No.	Initial config.	Point A (40,0,0°)	Point B (30,20,90°)	Point C (0,20,180°)
1	0	-41.8	-13.4	0
2	0	0	0	0
3	0	0	0	33.2
4	0	0	0	0
5	0	0	43	34.1
6	0	41.6	0	40.7
7	0	42	39.2	40.7
8	0	0	20.9	0
9	0	0	0	31.1
10	0	-41.4	0	0
Active joints	-	4	4	5
Δd [cm]	-	0.07	0.13	0.07
$\Delta\theta$ [deg]	-	-0.29	0.07	0.38
Distance travelled	-	50 cm	50 cm	50 cm
rotation		167°	117°	180 °
Conv. rate		69%	75%	84%

In the following example (Figure 8.1), we searched for a solution to three different target points with given orientations $X_A(40,0,0^o)$, $X_B(30,20,90^o)$, and $X_C(0,20,180^o)$. Starting from an initial configuration where the mobile actuator was at the origin and all the joint angles were 0^o, the algorithm success rate in finding a solution within the accepted range (position error < 0.2 cm and orientation error < 0.5 degrees) was 69% in A, 75% in B, and 84% in C. For point A, a solution was found by rotating only four joints and the errors were 0.07 cm and -0.29 degrees. In B, a solution was found by rotating only four joints and the error is 0.13 cm and 0.07 degrees. In C, five joints were rotated, and the error was 0.07 cm and 0.38 degrees. For each point, one of the results with the smallest number of actuated joints is presented in 0

6.2 Reaching a Target with Any Link (AL)

One of the unique features of the MASR robot is that its gripper can reach a specific target if any of the links is above or below the target (see

Figure 10 and video). This feature is especially useful if the target point is close to the base link or if the mobile actuator is required to move objects along the path of the links. If the target point is above or below a given link j, the distance from the line along (collinear) the link j to the target, denoted by d_{LINK}, must be zero. The target point must also be within the boundaries of the link; i.e., between joint j and j+1 (see Figure 9). We denote the distance between the target to adjacent joints by dj and d_{j+1}. In order to satisfy this condition, both distances must be simultaneously smaller than the length of the link L.

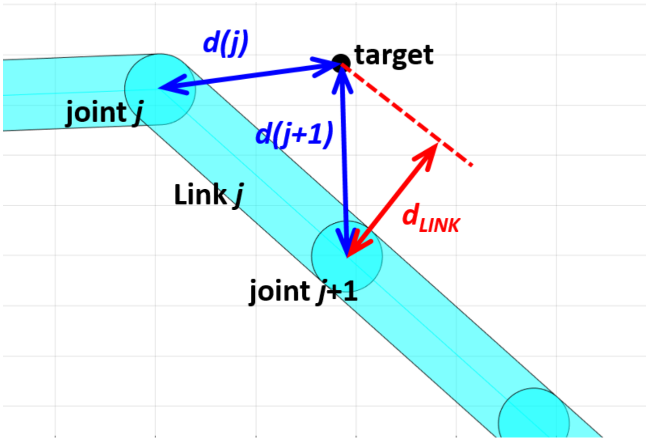

Figure 6.2. The distance of the target from link *j* and the adjacent joints (*j* and *j+1*).

The cost function in the AL case is defined as:

$$F\left(\Delta\boldsymbol{\theta}_{\mathbf{j}},\boldsymbol{\theta}_{\mathbf{i}},\mathbf{X}_{\mathbf{f}}\right)=f_{LINK}+f_{OR}+f_{STOPS} \tag{18}$$

where f_{OR} and f_{STOPS} are identical to the *LL* case, and f_{LINK} is defined as:

$$f_{LINK}=d_{LINK}{}^{2}+f_{JOINT}\left(j\right)+f_{JOINT}\left(j+1\right) \tag{19}$$

and the function f_{JOINT} is:

$$f_{JOINT}\left(j\right)=abs\left(L-d\left(j\right)\right)-\left(L-d\left(j\right)\right) \tag{20}$$

The cost function $f_{JOINT}(j)$ becomes zero if the distance between the joint to the target point is less than L and positive (linearly monotonous) if the distance is larger than L. Minimizing the combination of $f_{JOINT}(j)$, $f_{JOINT}(j+1)$, together with the distance d_{LINK} ensures that the target point is on the link j.

The results of the algorithm that found an optimal solution for the three points A,B and C (points identical to the previous section), are presented in

Figure 10 and summarized in 0The algorithm successfully found solutions at high convergence rates (respectively 96%, 84% and 98% for A, B and C). The solution for A is trivial and the mobile actuator travelled a distance of 40 cm along the links without rotating any joint. In B, the mobile actuator rotated only 3 joints and reached the point using its 9th link after travelling 45 cm. In C, the rotation of 5 joints was required and the robot reached the point with its 6th link.

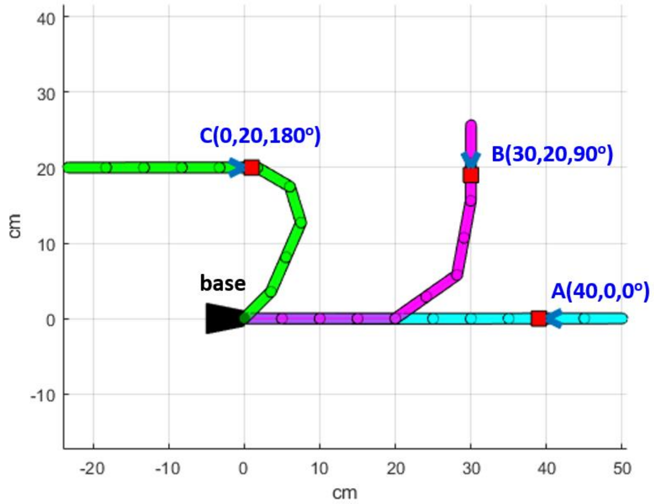

Figure 6.3. Starting at an initial configuration where all the joints were at 0 degrees, the robot reached points A, B, and C using the AL method.

Table 6.2: Solution for A, B, and C using the “AL” Method.

Joint No.	Initial config.	Point A (40,0,0°)	Point B (30,20,90°)	Point C (0,20,180°)
1	0	0.0	0.0	45.0
2	0	0.0	0.0	21.5
3	0	0.0	0.0	0
4	0	0.0	0.0	40.7
5	0	0.0	35.2	42.4
6	0	0.0	0.0	30.4
7	0	0.0	44.2	0
8	0	0.0	0.0	0
9	0	0.0	10.2	0
10	0	0.0	0.0	0
Active	-	0	3	5
Δd [cm]	-	0.00	0.004	0.006
Δθ [deg]	-	0.00	0.23	0.03
Travelled	-	40 cm	45 cm	30 cm
Rotation		0 °	90 °	180°
Conv.		96%	84%	98%

6.3 Comparing the LL and the AL Methods

In the previous section, the robot travelled from its original location (straight line where the mobile actuator was located at the origin O) to points A, B and C. In this section, we compare the distance travelled by the mobile actuator, the total angular rotation of the joints, the number of stops and the total time. Using Eq. (4) and assuming that V_m=20 cm/s and ω=360 degrees/s and that T_{stop}=0.1 s, the total time required for performing the mission can be calculated. A comparison between the two methods is presented in 0The results show that the AL method is substantially faster than LL (by 20% to 45%).

Next, we compared the two methods when performing consecutive tasks by travelling to the origin O and then to points A, B and C. The results of the comparison are presented in Figure 6.4 and Table 6.4.

Table 6.3: Comparing the Two Methods Reaching points A, B and C.

	Point A	**Point B**	**Point C**
Distance LL	45	45	45
Distance AL	40	45	25
Angular LL [deg.]	167	116	180
Angular AL [deg.]	0	90	180
Stops LL	5	6	7
stops AL	1	3	5
Total time LL [s]	3.7	3.5	4
Total time AL [s]	2.1	3	2.7

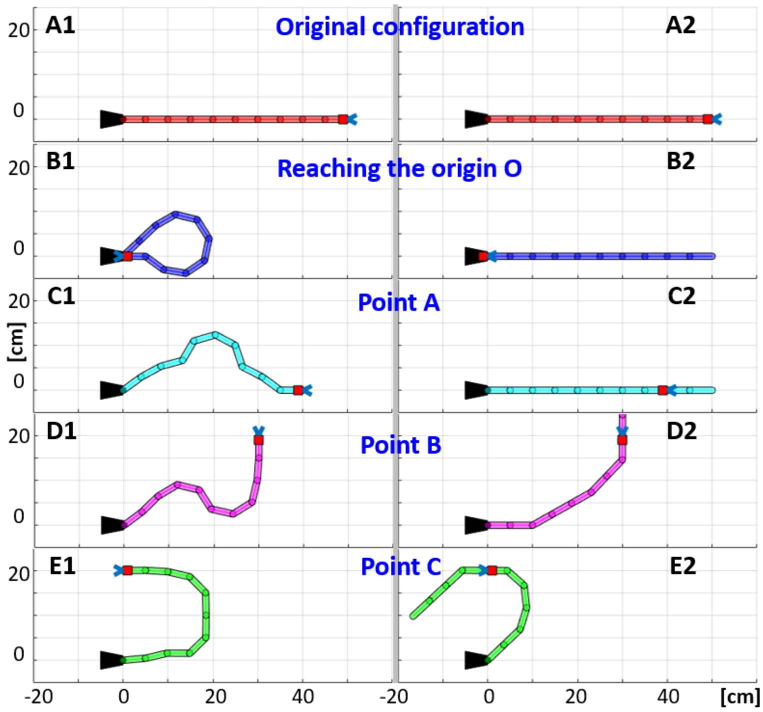

Figure 6.4. Comparison of the LL and AL methods performing consecutive tasks. Starting from its original configuration, the robot moves its mobile actuator to points O, A, B and C.

Table 6.4: Comparing the Two Methods when Travelling Along the Path OABC.

	O	OA	AB	BC	OABC
Distance LL [cm]	45	90	90	90	315
Distance AL [cm]	0	40	45	75	160
Angular LL [º]	339	209	333	266	1147
Angular AL[º]	0	0	90	133	223
Stops LL	8	5	7	7	27
stops AL	0	1	4	5	10
Total time AL [s]	4.9	6.2	7.1	6.7	24.8
Total time LL[s]	0	2.1	3.1	5	10.3

Starting from the original configuration “A1”, the robot in the LL case must rotate 9 of its joints to reach the origin “B1”, whereas in the AL method it does not rotate any joints at all “B2”. The same holds in case “C” as in the AL method, where the mobile actuator only needs to travel to link 8 without rotating any of its joints. In case “D2”, using the AL method, the target can be reached by only using 9 links and in “E2” by only using 6 links. 0presents the number of steps required and time elapsed for task performance. It shows that performing the task using the AL method is substantially faster (nearly 60%) and reduces the distance travelled by the mobile actuator and rotated joints.

7. Experiments and Results

This section presents the results of the experiments conducted with a 3D printed prototype of the robot. We tested its full functionality in multiple experiments which included reaching different points in 3D space, picking up objects with the mobile actuator, translating them using the mobile actuator while travelling over the links and releasing them at the target points. The experiments were pre-planned offline using our optimization algorithm and performed automatically using the robot (see video).

7.1 Reaching a Target Over an Obstacle

The first experiment using this robot mimicked picking a piece of fruit from a tree and placing it in a basket. Starting at A, the vertical actuator raises the arm by 26 cm while the mobile actuator advances slightly towards the ball "B" hanging from the top with a nylon wire. The mobile actuator grasps the ball in "C" and advances to the 5th joint while rotating it by 4 degrees "D". Then, the mobile actuator advances to the 6th joint while rotating it by 24 degrees "E" and continues towards the 10th link to drop the ball into the target bowl "F". See attached video.

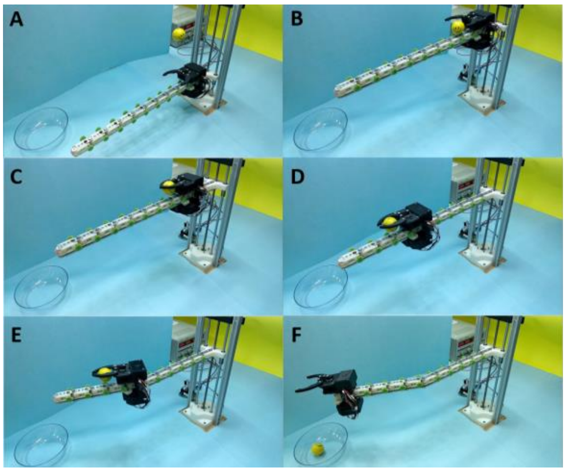

Figure 7.1. The MASR robot picks a ball hanging from the top, translates it along the links and drops it into a basket.

7.2 Relocating an Object

In this experiment, the robot's task was to move the position of a cup using a minimal number of joints. The origin and target locations of the cup were at different heights. Starting in "A", the linear vertical actuator raises the arm by 10 cm. Moving forward, the mobile actuator advances to the 7th and the 8th joints and rotates their angles by 28 and 16 degrees respectively "B". Then, the mobile actuator continues advancing along the links to reach cup "C". After grasping the cup, the linear vertical actuator raises the arm by 12 cm, while the mobile actuator returns to the 8th link "D" and rotates it into negative 16 degrees and the 7th link into negative 28 degrees "E". The mobile actuator then moves along the links and places the cup in the target location "F". See attached video.

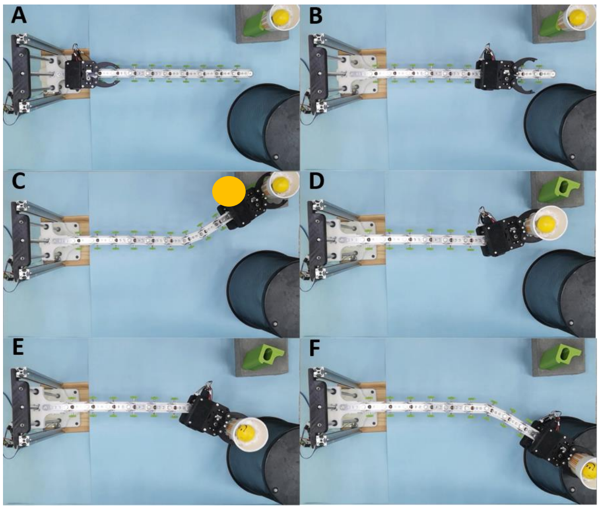

Figure 7.2. Starting from a straight configuration, the MASR relocates the cup.

7.3 Reaching Around an Obstacle

In the last experiment presented here, the mobile actuator rotated the links to go around an obstacle (simulating a wall) to reach the target. The wall was 7 cm away in the *y* direction from the origin of the robot and was 25 cm long (from *x*= 0 to *x*=25 cm). The target location was (10,-20). Starting from straight configuration "A", the mobile actuator travels toward the 8th joint ("B" to "D") and rotates the joits [(5,-38°) (6,-39°) (7,-38°) (8,-35°)] as it advances. Then the mobile actuator proceeds to the last link "E" and releases the ball "F". See attached video.

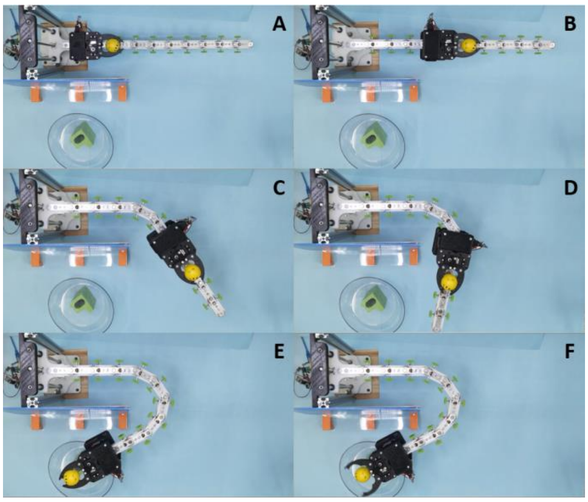

Figure 7.3. Starting from straight configuration, the MASR rotates its links to turn around an obstacle.

8. Summary and Conclusions

In this paper, we presented a novel serial robot composed of a multi linkage arm with passive joints and a mobile actuator that can travel along the arm and rotate the links. The mobile actuator is fitted with a gripper that allows it to grasp objects along its path and translate them quickly along the arm. This design makes it possible to reduce the size of the robot, its weight and simplify its design. As it has no wiring along the links, the links can be easily replaced and their size and number simply changed according to the requirement of the task. The mobile actuator can also be replaced, and more than one mobile actuator can be used.

We developed a locomotion algorithm based on optimizing a time-based function to minimize the operation time and actuation of the robot. Since our gripper can be moved along the links, we compared the time requirements for a task in which the robot relocates an object from one point to another with a given orientation for two situations: 1) the gripper can only grasp an object when the gripper is at the last link "LL". 2) The gripper can grasp objects at any link along the arm "AL". A comparison of the time elapsed in each of the two methods shows that in the second case, the time can be reduced by nearly three-fold.

Finally, we developed an experimental prototype of the robot which can automatically perform its pre-planned tasks. We used the robot to demonstrate multiple tasks which include relocating objects by rotating a minimal number of joints and translating objects along the robot's arm.

Note that while this robot is very simple and lightweight, it is substantially slower than regular fully actuated serial arms. Therefore, this robot should be used in applications where high speed is not required such as space applications, agriculture, maintenance, painting and search and rescue operations, for example.

Our future work will focus on using multiple mobile robots, improving the design and the mobility of the MASR in 3D space and developing a motion planning algorithm based on reinforcement learning.

Appendix A – Video Link

https://drive.google.com/file/d/1PNIf69e3unfYtujQpRS_nlFsFOV-IRa6/view?usp=sharing

Appendix B – Transmission Ratio

In order to find the robot's angular displacement resolution, the rotational gear transmission ratio was needed to be calculated. A complete revolution of the motor's shaft ends up with a complete revolution of the partial gears. Since the partial gears rotate the links' spur gears, and the last are fixed to the worm module via a shaft, the rotational transmission will be calculated as follows:

$$i_{rot\_sys} = \frac{Z_{partial\_gear}}{Z_{link\_gear}} \cdot \frac{Z_{worm}}{Z_{worm\_gear}} \qquad (A.1)$$

Where $Z_{partial\_gear}$ is the number of teeth of the partial gear, Z_{link_gear} is the number of teeth of the spur gear attached at the both sides of the links, Z_{worm} is the number of teeth of the worm module, and Z_{worm_gear} is the number of teeth of the printed worm gear. Applying the values end up with:

$$i_{rot\_sys} = \frac{4}{12} \cdot \frac{1}{38} = \frac{1}{114} \qquad (A.2)$$

For a complete round of the rotation motor, we will receive $1/114$ round of the worm gear. From Eq. (A.2) we derive the relative angle displacement for every spin of the motor:

$$\theta_{resolution} = i_{rot\_sys} \cdot 360 = \frac{360}{114} \approx 3.2 \deg \qquad (A.3)$$

Since the partial gears can be disconnected from the link's spur gears twice over one spin of the rotational motor, we can in fact gain control over 1.6° degrees of the angle displacement.

Appendix C – Structural Rigidity

The serial arm is experiencing a deflection as a function of the distance from the base link. This deflection is due to the weight of the links, the weight of the mobile actuator, and the payload carried by the gripper. We tried to find an approximation to the deflection, depends on the number of links of the serial arm. in order to perform the calculations, we have made some assumptions:

- The base link is rigidity connected to the vertical driving mechanism, as it can carry bending moments.
- The links are rigidity connected to each other, as a one unit.
- For calculating the moment of inertia I and the young's modulus E, the area of the cross-section was considered as constant and not as function of x.

Due to the above assumptions, we can relate to this problem as a cantilever beam which experienced two vertical forces (see Fig. B.1). The first one is a uniform distributed load, caused by the links' weight, and can be converted to a force that acts at the COM (Center of Mass) of the beam. The second force is derived from the mobile actuator weight and the payload acts on it. We would like to examine the extreme case while the actuator is located on the tip of the last link of the beam.

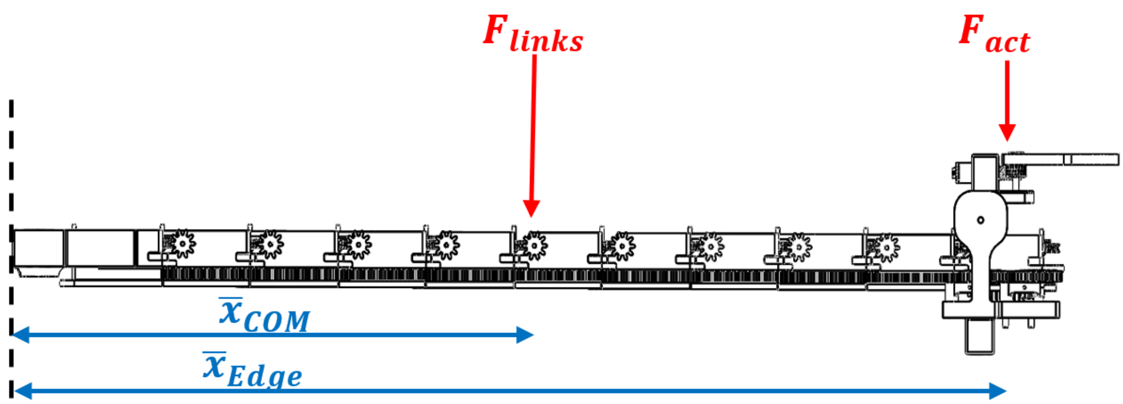

Figure B.1. A side view of MASR robot as a uniform cantilever beam, which is experiencing two vertical forces.

The COM is:

$$\bar{x}_{COM} = 0.5 \cdot n \cdot L \qquad (B.1)$$

Where n is the number of links in the kinematic chain including the base link (since the length of the links and the base link is equal), and L is the length of an individual link. The edge location of the kinematic chain is:

$$x_{Edge} = n \cdot L \qquad (B.2)$$

To find the deflection, we use the Newton's first law. First, we will find the reactions (moment and forces) acting at the fixed edge of the beam, known as point A. Assuming quasi-static motion, the sum of moments relative to the fixed-point A yields:

$$\sum M = M_A - (n \cdot F_{link}) \cdot \bar{x}_{COM} - F_{act} \cdot x_{Edge} = 0 \qquad (B.3)$$

Where M_A is the bending moment acting at point A, F_{link} is the force due to the load caused by the link's weight, and F_{act} is the force due to the actuator's weight plus the payload. Using Eq. (B.1) and (B.2), and after some arrangements, (B.3) becomes:

$$M_A = 0.5Ln^2 \cdot F_{link} + Ln \cdot F_{act} \qquad (B.4)$$

The net force in the vertical direction is:

$$\sum F_y = F_{y_A} - (n \cdot F_{link}) - F_{act} = 0 \qquad (B.5)$$

Where F_{y_A} is the vertical force acting at point A. After some arrangements (B.5) becomes:

$$F_{y_A} = n \cdot F_{link} + F_{act} \qquad (B.6)$$

In order to calculate the beam deflection, we made some assumptions:

- The beam experiences only linear elastic deformation
- The ratio of the beam's length to height is greater than 10

- Only small deflections are considered

Under the above assumptions, the equation governing the beam's deflection $y(x)$, can be approximated as:

$$\frac{d^2y(x)}{dx^2} = \frac{M(x)}{EI} \tag{B.7}$$

where the second derivative of its deflected shape with respect to x is interpreted as its curvature, E is the Young's modulus, I is the moment of inertia of the cross-section, and $M(x)$ is the internal bending moment.

We will find the deflection by performing an integral from order 2 and 1 on Eq. (B.7), receiving (B.8) and (B.9) with respect to x, interpreted as the beam's angle and deflection, respectively:

$$\frac{dy(x)}{dx} = \left(\int \frac{M(x)}{EI}\right) + c_1 \tag{B.8}$$

$$y(x) = \left(\int\int \frac{M(x)}{EI}\right) + c_1(x) + c_2 \tag{B.9}$$

In order to calculate the internal bending moment $M(x)$, we divided the beam into two segments; before (I) and after (II) the COM, where the load F_{links} is acting. After applying the internal bending moment of each segment into (B.8) and (B.9) separately, we will handle 4 different equations with 4 constants; c_1, c_2, c_3 and c_4. To find the constants, we use the following boundary conditions:

- Both angle and the deflection at the fixed-point A are equal to zero.
- At the COM, where the load F_{links} is acting, the beam fulfills continuity regarding both, the angle and the deflection.

Section I: from point A to COM

From left to right, the sum of moments in section I will be:

$$\sum M = M_I(x) + M_A - F_{y_A} \cdot x = 0 \qquad (B.10)$$

Where $M_I(x)$ is the internal bending moment developed in section I of the beam. Inserting (B.4) and (B.6) into (B.10):

$$M_I(x) = (n \cdot F_{link} + F_{act}) \cdot x - (0.5Ln^2 \cdot F_{link} + Ln \cdot F_{act}) \qquad (B.11)$$

Inserting (B.11) into (B.8) and (B.9), and after applying the boundary condition for calculating the constants, we receive:

$$y_I(x) = \frac{1}{EI}\left[\frac{(n \cdot F_{link} + F_{act})}{6}x^3 - (0.5Ln^2 \cdot F_{link} + Ln \cdot F_{act})x^2\right] \qquad (B.12)$$

Section II: from COM to the free edge

From left to right, the sum of moments in section II will be:

$$\sum M = M_{II}(x) + M_A - F_{y_A} \cdot x + n \cdot F_{link} \cdot (x - 0.5Ln) = 0 \qquad (B.13)$$

Where $M_{II}(x)$ is the internal bending moment developed in section II of the beam. Inserting (B.4) and (B.6) into (B.13):

$$M_{II}(x) = F_{act} \cdot x - Ln \cdot F_{act} \qquad (B.14)$$

Inserting (B.14) into (B.8) and (B.9), and after applying the boundary condition for calculating the constants, we receive:

$$y_{II}(x) = \frac{1}{EI}\left[\frac{F_{act}}{6}x^3 - \frac{Ln \cdot F_{act}}{2}x^2 - \frac{L^2n^3 \cdot F_{link}}{8}x + \frac{L^3n^4 \cdot F_{link}}{48}\right] \qquad (B.15)$$

In order to find an approximation for Young's modulus, we will use Voigt model for composite materials, while the aluminum support is acting as the fibers of the composition. If we will consider the composite material under uniaxial tension, we can use Hooke's law:

$$E = \frac{\sigma}{\varepsilon} = \frac{F}{A\varepsilon} \qquad (B.16)$$

$$F = AE\varepsilon \qquad (B.17)$$

Where F is the uniaxial force applying on the composite material, A is the cross-section area, and ε is the strain.

Applying the force balancing equation, we will receive:

$$A_c E_c \varepsilon_c = A_f E_f \varepsilon_f + A_p E_p \varepsilon_p \qquad (B.18)$$

Where f represents the fibers, p represents the printed material and c represents the composite material contains both the fibers and the printed material.

If both the materials is to stay intact, the strain of the fibers, ε_f must equal to the strain of the matrix, ε_m must equal to the strain of the composition, ε_c. The area of the cross section is the summation of the fibers area plus the matrix area. Thus:

$$E_c = \frac{A_f}{(A_f + A_p)} E_f + \frac{A_p}{(A_f + A_p)} E_p \qquad (B.19)$$

If the relative area of the printed material is 0.94, the Young's modulus of the printed material is $E_p = 2[Gpa]$, and the Young's modulus of the aluminum is $E_f = 68.9[Gpa]$, then the Young's modulus of the composite material is:

$$E_c = 6[Gpa] \qquad (B.20)$$

The inertia moment of the cross-section is:

$$I_y = 2.44 \cdot 10^{-8} [m^4] \qquad (B.20)$$

Appendix D – Deflection Due to Tolerances

The serial arm is experiencing another deflection due to the robot's tolerances. As described in Fig. C.1, the connection between two parallel links are made by aluminum axis. Due to the printer properties and due to the fact that the connection involves two different materials, the hall was made by tolerance of +0.1mm greater than the aluminum axis.

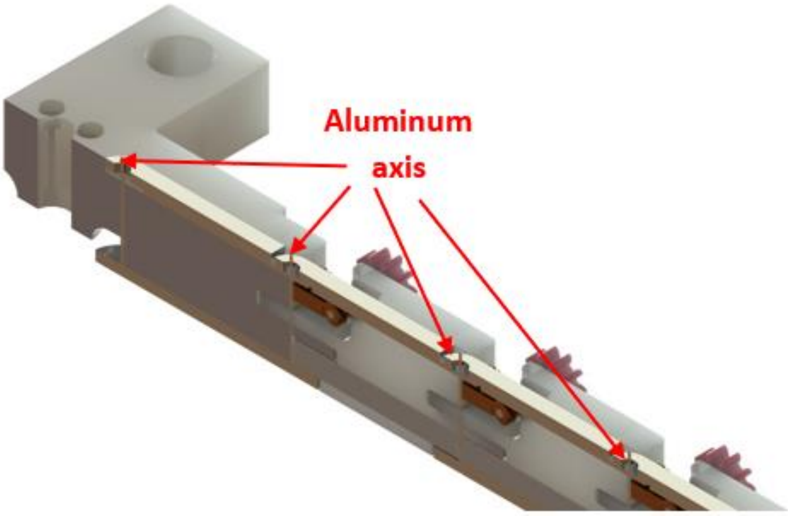

Figure C.1. A section view of the serial arm.

From Fig. C.2 we can notice that the angle deflection γ between two parallel links will be greater by γ from the previous one. Meaning, we can relate this problem as a series while the first element is γ and the difference is also γ.

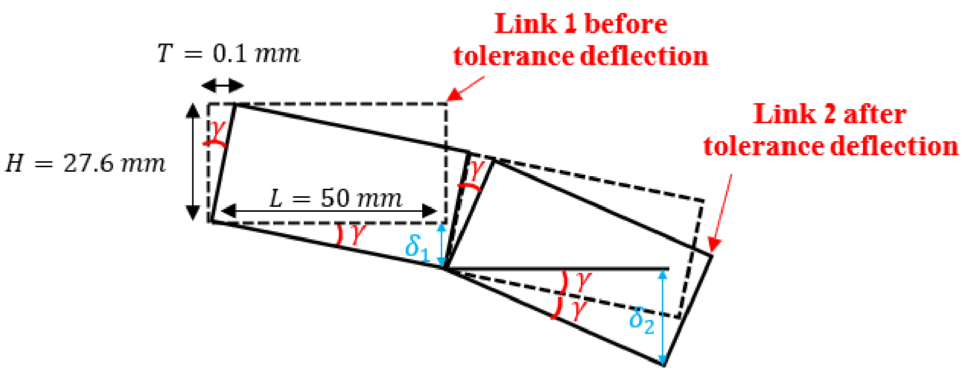

Figure C.2. A schematic description of the tolerance deflection.

For calculating this problem, we will assume very small deflections, thus:

$$sin_{\gamma} = tan_{\gamma} \approx \gamma \qquad (C.1)$$

The angle and the deflection of link 1 in a relation to the horizontal plane will be:

$$sin_{\gamma} \approx \gamma = \frac{T}{H} = 3.6 \cdot 10^{-3} rad \qquad (C.2)$$

$$\delta_1 = \theta \cdot L = 0.18\, mm \qquad (C.3)$$

The deflection of link 2 in a relation to the horizontal plane will be:

$$\delta_1 = 2\theta \cdot L = 0.36\, mm \qquad (C.4)$$

The deflection of link *n* will be:

$$\delta_n = n \cdot \theta \cdot L \qquad (C.5)$$

The total deflection *n* links will be:

$$\delta_n = \sum_{i=1}^{n} n \cdot \theta \cdot L \qquad (C.6)$$

The total deflection 10 links will be:

$$\delta_{10} = \sum_{i=1}^{10} n \cdot \theta \cdot L = 9.9\, mm \qquad (C.7)$$

Appendix E – External Forces Durability

While applying external forces on the serial arm, the worm gear transmission may experience fraction. In order to calculate the allowable force over the horizontal plane without leading to a mechanical failure, we conducted an experiment while loading two parallel links until we experienced fraction (see Fig. D.1).

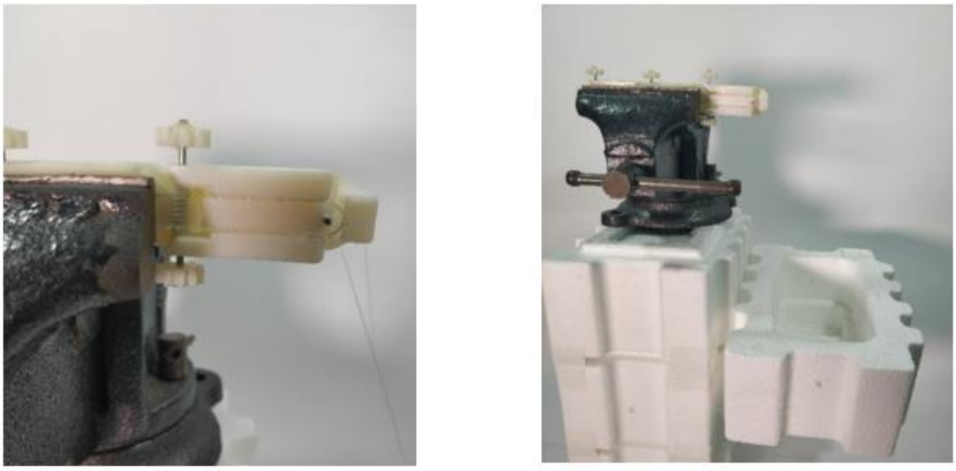

Figure D.1. Experimental system.

The experiment was conducted over two links in order not to ruin more links. By a simple calculation we can translate the experiments outcomes over the original arm which is composed from 10 links. Logically, the first worm gear to experience mechanical failure will be the first one along the kinematic chain due to the distance from the force. Fig. D.2 describing the forces and torques over the experimental model.

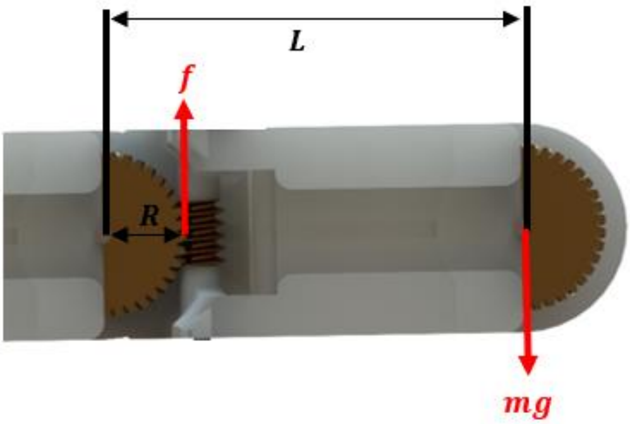

Figure D.2. Forces and torques over the experimental model.

From torques equilibrium:

$$f_{max} \cdot R = mg \cdot L \tag{D.1}$$

While m is the load, L is the distance between the center of the first worm gear to the load, f is the force acting on the first worm gear and R is the distance to the force.

Appendix F – Motion Planning Codes

Optimization:

```
% This function finds the optimal path pf MASR robot to a specific
% (arbitrary) point in the xy plan according to the cost function

close all;
clear all;
clc;


N=10; L=5;
T_V=zeros(1, 10);
T0_V=zeros(1,N)+0*pi/2*(rand(1,N)-0.5)
DT_V=sym('DT',[1 N])
XT=[0 20]*1;
ThetaT=pi;

UB = ones(N,1)*(pi/4)*1.05;    % UB(N)=UB(N)*0.01
LB = ones(N,1)*(-pi/4)*1.05;   % LB(N)=LB(N)*0.01


X_V=zeros(2,11);
for i=1:N;
    X_V(:,i+1)=X_V(:,i)+L*[cos(sum(T0_V(1:i))) ; sin(sum(T0_V(1:i)))]
end
for i=1:N;
    line([X_V(1,i) X_V(1,i+1)] , [X_V(2,i) X_V(2,i+1)])
end
hold on; plot(X_V(1,:),X_V(2,:),'o'); axis equal
hold on; plot(XT(1), XT(2), 'x')

XS_V=L*[cos(sum(DT_V(1:1)));sin(DT_V(1:1))];
for i=2:N;
    XS_V(:,i)=X_V(:,i-1)+L*[cos(sum(DT_V(1:i)));sin(sum(DT_V(1:i)))]
end

color = cell(1,2);
color{1}='c';
color{2}='m';
color{3}='g';

i=N;

cost_function1=inline('norm(XT-L*[sum(cos(cumsum(DT_V+T0_V)))
sum(sin(cumsum(DT_V+T0_V)))])','XT', 'T0_V','DT_V','i','L')
cost_function2=inline('sum(abs(DT_V)>0.01)', 'DT_V')
cost_function3=inline('1-sum(abs(DT_V).^5)', 'DT_V')
cost_function4=inline('sum(abs(DT_V).^0.02)', 'DT_V')
%cost_function5 is a seperate function
cost_function6=inline('abs(norm(XT-L*[sum(cos(cumsum(DT_V+T0_V)))
sum(sin(cumsum(DT_V+T0_V)))])-L) + norm(XT-
L*[sum(cos(cumsum(DT_V+T0_V))) sum(sin(cumsum(DT_V+T0_V)))])-L','XT',
'T0_V','DT_V','i','L')
cost_function7=inline('abs(norm(XT-L*[sum(cos(cumsum(DT_V(1:i-
1)+T0_V(1:i-1)))) sum(sin(cumsum(DT_V(1:i-1)+T0_V(1:i-1))))])-
L)+(norm(XT-L*[sum(cos(cumsum(DT_V(1:i-1)+T0_V(1:i-1))))
```

```
sum(sin(cumsum(DT_V(1:i-1)+T0_V(1:i-1))))])-L)','XT',
'T0_V','DT_V','i','L')
cost_function8=inline('sum(abs(DT_V).^0.5)', 'DT_V')
cost_function9=inline('200*(sum(DT_V)-ThetaT)^2', 'DT_V', 'ThetaT')
%funtion is one if error is 0.2 degrees

%joint position
W1=1*1; W2=1*0; W3=1; W4=1*0; W5=1*0; W6=1*0; W7=1*0; W8=1; W9=1;
%link position
W1 =1*0; W2=1*0; W3=1; W4=1*0; W5=1*1; W6=1*1; W7=1*1; W8=1; W9=1;


DT0_V=(rand(1,N)-0.5)*pi/2;
fun=@(DT_V)(W1*cost_function1(XT,T0_V,DT_V,i,5)+W2*cost_function2(DT_
V)+W3*cost_function3(DT_V)+W4*cost_function4(DT_V)+
W5*distance_to_link(XT,L,i,T0_V,DT_V))+W6*cost_function6(XT,T0_V,DT_V
,i,5)+W7*cost_function7(XT,T0_V,DT_V,i,5)+W8*cost_function8(DT_V)+W9*
cost_function9(DT_V, ThetaT);


trials=100;

for j=1:trials;
    [theta,fval]=fmincon(fun,DT0_V,[],[],[],[],LB,UB,[],[]);
    active_joints_V(j)=sum(abs(theta)>0.01);
    DT_M(:,j)=theta';
    fval_V(j)=fval;
    error_V(j)=norm(XT-L*[sum(cos(cumsum(theta+T0_V)))
    sum(sin(cumsum(theta+T0_V)))]);
    DT0_V=(rand(1,N)-0.5)*pi/4;
    distance_V(j)=distance_to_link(XT,L,i,T0_V,theta)

    active_joints_V(j)=sum(abs(theta)>0.01)+100*(distance_V(j)>0.2)+
    100*((sum(theta)-ThetaT)^2>7.6e-5);
end

[Min_val,Min_index]=min(active_joints_V);
TF_V=DT_M(:,Min_index)';

figure(10);

T_V(1:N)=TF_V;
TF_V=T_V
MASR_Path(TF_V,L,color{1});
plot_motor(XT(1)-L*cos(sum(TF_V)),XT(2)-L*sin(sum(TF_V)),sum(TF_V));

hold on;
plot(X_V(1,:),X_V(2,:),'o');
axis equal;
hold on;
plot(XT(1), XT(2), 'x','markersize',10, 'linewidth', 2,'color','k');

%The data of the chosen path
fval                                %The value of the cost function
Min_val                             %Number of joints to be rotated
distance=distance_V(Min_index)      %The distance from the target
angle_change=DT_M(:,Min_index)      %The values of the angles
%The angle's error from the target
total_angle_error_deg=(sum(angle_change)-ThetaT)*180/pi
rejected_sol=sum(active_joints_V>100) %Number of rejected solutions
```

MASR Path:

```
function [path,x,y] = MASR_Path(theta,l,color)
%this function receives the angles arrangement in the kinematic
%chain (theta), the length of each link (l), the color definition.
%this function plot the   MASR path (link configuration).

N = numel(theta);                %number of links
x = zeros(1,N+1);                %x location of each link
y = zeros(1,N+1);                %y location of each link
mat = zeros(4,4,N);
fin_mat = 1;

%%Danavit-Hartenberg matrix
for i = 2:N+1
    mat(:,:,i)=[cos(theta(i-1)) -sin(theta(i-1)) 0 l*cos(theta(i-1));
                sin(theta(i-1)) cos(theta(i-1)) 0 l*sin(theta(i-1));
                0 0 1 0;
                0 0 0 1];
    fin_mat = fin_mat * mat(:,:,i);
    x(i) = fin_mat(1,4);
    y(i) = fin_mat(2,4);
end

axis equal;
grid on;
hold on;
path = 0;
path = line(x,y,'linewidth',0.5,'color',color);       %link
configuration plot

%The MARS path
rd = 1;
w = 2;
abs_angle = cumsum(theta);
t1 = -pi/2:0.01:pi/2;
t2 = pi/2:0.01:3*pi/2;
x1 = (rd/sqrt(2))*cos(t1);
y1 = (rd/sqrt(2))*sin(t1);
base = patch([-l 0 x1 0 -l],[w rd y1 -rd -w],'k');      %  base link
x1 = 0;  y1 = 0;
x2 = 0;  y2 = 0;
ang1 = 0;  ang2 = 0;
for i = 1:N
    ang1 = t1+abs_angle(i);
    ang2 = t2+abs_angle(i);
    x1 = (rd/sqrt(2))*cos(ang1)+x(i);
    y1 = (rd/sqrt(2))*sin(ang1)+y(i);
    x2 = (rd/sqrt(2))*cos(ang2)+x(i);
    y2 = (rd/sqrt(2))*sin(ang2)+y(i);
    xdata = [x1+l*cos(abs_angle(i)) x2];
    ydata = [y1+l*sin(abs_angle(i)) y2];
    patch(xdata,ydata,color,'FaceAlpha',.5);
end

end
```

Plot Motor:

```
function [p,line1,line2] = plot_motor(X,Y,T)
%this function plots the motor's location and orientation

Xcube=[1 3 3 1]+2;
Ycube=[-1 -1 1 1];
XYcube=[Xcube; Ycube];
Xline1=[3 5]+2; Xline2=[3 5]+2;
Yline1=[0 -1]; Yline2=[0 1];
XYline1=[Xline1;Yline1];
XYline2=[Xline2;Yline2];

R_M=[cos(T) -sin(T) ; sin(T) cos(T)];

XYcube=R_M*XYcube;
XYline1=R_M*XYline1;
XYline2=R_M*XYline2;



p=patch(X+XYcube(1,:),Y+XYcube(2,:), 'r');
line1=line(X+XYline1(1,:), Y+XYline1(2,:),'linewidth',4);
line2=line(X+XYline2(1,:), Y+XYline2(2,:),'linewidth',4);

axis equal;

end
```

Appendix G – Work Article

Design and Modelling of a Minimally Actuated Serial Robot

Yotam Ayalon, Lior Damti and David Zarrouk

***Abstract*—In this paper we present a minimally actuated overly redundant serial robot (MASR). The robot is composed of a planar arm comprised of ten passive rotational joints and a single mobile actuator that travels over the links to reach designated joints and rotate them. The joints remain locked, using a worm gear setup, after the mobile actuator moves to another link. A gripper is attached to the mobile actuator thus allowing it to transport objects along the links to decrease the actuation of the joints and the working time. A linear stepper motor is used to control the vertical motion of the robot in 3D space. Along the paper, we present the mechanical design of the robot with 10 passive joints and the automatic actuation of the mobile actuator. We also present an optimization algorithm and simulations designed to minimize the working time and the travelled distance of the mobile actuator. Multiple experiments conducted using a robotic prototype depict the advantages of the MASR robot: its very low weight compared to similar robots, its high modularity and the ease of replacement of its parts since there is no wiring along the arm, as shown in the accompanying video.**

***Index Terms*— Serial robot, Minimal actuation, Mobile actuator, Mechanical design.**

INTRODUCTION

Conventional serial robots are composed of several rigid links connected to each other using actuated joints. Most 3-dimensional commercially available serial robots have between 4 and 7 degrees of freedom. In tasks that call for maneuvering in confined spaces, traditional serial robots are often insufficient. In some industries the inability to do certain tasks because of restricted access has major commercial significance.

The prime reason for developing hyper redundant robots (alternatively known as snake robots), is their ability to navigate around obstacles and in highly confined spaces. They are typically actuated using 10 to 20 motors [32]-[50]. Extensive research over the past several decades has generated many different configurations and mechanisms for a variety of applications such as search and rescue operations [52]-[60], as well as maintenance and medical applications for minimally invasive procedures [61]-[66]. Due to their relatively low weight, these robots [67]-[39] as well as continuum robots [23] are possible candidates for planetary exploration and space satellite maintenance.

Control and motion planning with serial robots nevertheless present formidable challenges in terms of high dimensionality analysis. Numerous researchers have addressed the planning problem using different optimization strategies that have led to substantial advances [24]-[28].

To simplify the kinematics and actuation, and minimize the dynamic modeling, we suggested in previous works a minimally actuated reconfigurable track robot [32], and a preliminary design concept serial robot with a mobile actuator MASR which travels along the links to rotate the joints [33]. The MASR incorporates multiple characteristics and advantages from both minimally actuated robots and hyper redundant robots. The smaller number of motors and the simplicity of the design allow for increased reliability, smaller weight, lower costs and high modularity.

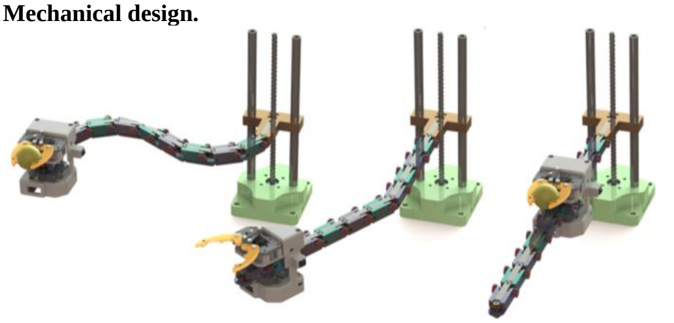

Figure 2. The minimally actuated serial robot MASR is a newly developed robot with a large number of joints and a single mobile actuator. The mobile actuator travels along the links to actuate the joints.

Here we extend on these works [32][33] and present a newer version of the MASR robot with multiple mechanical improvements which increase its strength and accuracy. The arm is now actuated vertically using a screw lead (enabling 3D motion) and the rotation of the joints is performed using worm gears which provide higher torques accuracy. The mobile actuator is now fitted with a gripper which is used to effectively translate objects along the links without having to rotate the arm. We also developed an electronic controller to automatically and more precisely control the vertical position of the arm and the translation of the mobile actuator and rotation of the links using sensors. Finally, we present a motion planning for the case in which the mobile actuator grasps objects along the tip of the arm only and for the case in which the mobile actuator can carry objects along the links.

This paper is organized as follows: The design of the robot is presented in Section II. Section III deals with the kinematic analysis. Section IV focuses on developing a motion algorithm that reduces the working time and the travelled distances of the actuators. In Section V, multiple experiments performed using the robot are presented.

ROBOT DESIGN AND ACTUATION

The MASR robot presented in this paper (Figure 3) is composed of a serial planar arm with 10 joints, a linear actuator that can displace the arm in the vertical direction and a mobile actuator that can travel along the links and rotate the joints when needed. Considerable effort was invested in keeping the

D. Zarrouk and Y.Ayalon are both associated with the department of Mechanical Engineering at the Ben Gurion University of the Negev, Israel. (zadavid@bgu.ac.il).

design of the robot as simple as possible and reducing its weight. The main characteristics of the first prototype are presented in 0

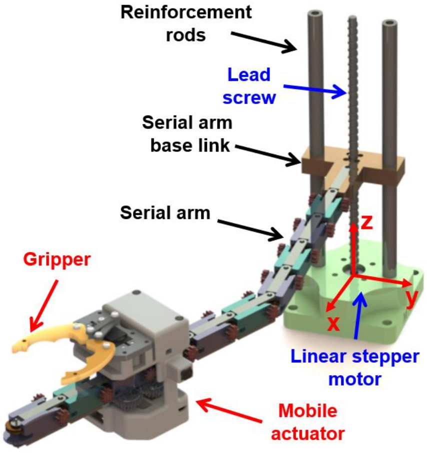

Figure 3. The mechanical design of MASR robot. The robot consists of a planar serial arm with 10 passive joints actuated by a mobile actuator. The mobile actuator that can travel over the links is fitted with a gripper to carry objects along its path. The vertical motion is actuated by a linear stepper motor.

Robot Design

The Serial Arm

The serial arm of the current design is composed of 10 identical links (Figure 4). The links are 5 cm long and 2 cm wide and are attached to each other through rotational joints. The length of the arm fitted with 10 links is 50 cm and its weight is 0.35 kg. A worm gear transmission is used to rotate the joints at a ratio of 1:38. The worm gear ensures that the links remain locked at the desired angle after the actuation is completed. The relative angle θ_j between two adjacent links (j-1 and j) can be varied in the range of [-45º, 45º].

At their bottom, the links have a gear rack designed to increase the traction of the mobile actuator when traveling over the links and to eliminate the possibility of sliding. In order to increase the rigidity of the 3D printed (plastic) links, aluminum supporting rods were added at their top and bottom. The weight of each link including the aluminum support is 30 grams. This 3D printed version of the robot is designed for a vertical workload of 0.5 kg. A workload of 0.5 kg causes a deformation of nearly 0.5 cm. Magnets were attached at the center of the joints to help the mobile actuator identify its location while travelling along the arm.

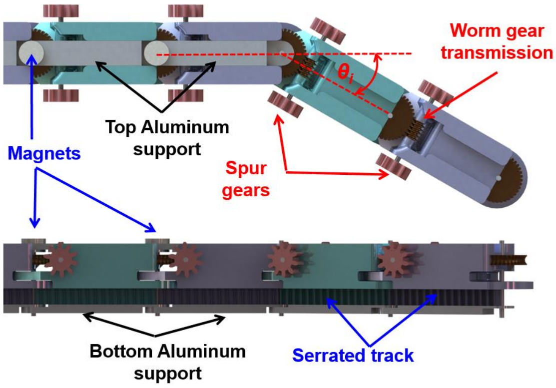

Figure 4. The robotic arm is composed of 10 links attached through rotational joints. A worm gear transmission is used to actuate the links and ensure that the relative angle is preserved when the mobile actuator departs from the joint.

The Mobile Actuator

The mobile actuator, presented in (Figure 5), is designed to travel over the links, stop at a designated location to rotate the joints and grasp objects using the gripper. It is composed of three separate mechanisms: the locomotive, the joint rotation mechanism and the gripper.

The Locomotive

The locomotive carries the actuator along the links using four serrated wheels. Two of the wheels on the one side are actuated using a rotational motor and the other two wheels, located on the other side, are passively actuated. To enable the locomotive to travel over curved joints (up to 45 degrees), the axes of the passive wheels are fixed on a rotational joint. This joint is fitted with springs, allowing the wheels to conform to the variation in the track and apply a gripping force on the tracks of the links.

The Joint Rotation Mechanism

The mobile actuator is fitted with a spur gear with partial gearing. When the mobile actuator reaches a specific link j, it engages the spur gear of the joint/link and rotates it. As a result, the relative angle between the two adjacent links (j and j-1) is changed (see Figure 5 and video). The partial gearing (four teeth per revolution) of the rotation mechanism is used to avoid unwanted collisions between the spur gear of the locomotive and links as the mobile actuator travels along the arm. The worm gear assembly has a ratio of 1:38, and the spur gear's ratio is 1:3, so that each full revolution of the partial spur gear will result in a 3.2 degrees rotation of the joint.

The Gripper

The gripper, attached to the mobile actuator, is an off-the-shelf two-finger mechanism actuated by a servo motor. It can hold objects at widths of 2.5 cm to 10.5 cm. Note that in this robot, the gripper is not fixed to the last link of the robot but rather to the mobile actuator. As a result, the mobile actuator can travel over the links to grasp objects and translate them along the arm. More sophisticated grippers with more fingers can be attached to the mobile actuator if needed. The gripper can also be replaced with a welding tool, a saw, or a paint brush for example, depending on the application requirements.

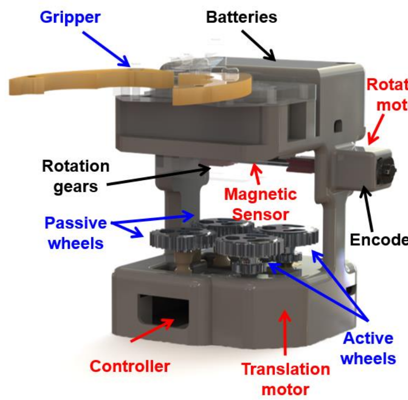

Figure 5. The mobile actuator is composed of a locomotive mechanism, a rotation mechanism and a gripper. The mobile actuator holds its controller and batteries onboard.

The Vertical Driving Mechanism

Vertical motion (z direction) is enabled by a lead screw rotated with a stepper motor located at the base of the robot. The diameter of the screw is 8 mm and its pitch 8 mm. Because the stepper motor makes 200 steps per revolution, the nominal accuracy of the motion is 0.04 mm. To reinforce the structure to prevent bending, two 10 mm steel rods are attached to the base of the robot (Figure 3). The total range of the vertical motion is 38 cm.

Manufacturing

The robot is mostly manufactured from 3D printed materials. The links, which require high resolution, were printed using a Polyjet printer (Object Connex 350) and the mobile actuator was printed using an FDM printer. To increase the strength of the serial arm and minimize bending, 3 mm thick aluminum rods were attached on the top and bottom of the links. Since there is no wiring along the links, their replacement is very simple.

CHARACTERISTIC PARAMETERS OF THE ROBOT.

rial arm Length (10 links)		50 cm
rial arm weight (10 links)		0.35 kg
obile actuator weight		0.3 kg
nt rotation speed		15 degrees/s
obile actuator speed		12.5 cm/s
rtical speed		10 cm/s
rtical workload		0.5 kg
le forces		0.1 kg
ecision		0.5 cm

Actuation and Control

Actuation

The MASR robot, including its gripper, is actuated using a total of four motors:

- One 12 V stepper motor to move the arm in the vertical direction. The stepper motor produces a torque of 36 Ncm. For the given lead screw diameter and pitch (both 8 mm) and assuming that the coefficient of friction is 0.3, the motor and lead screw setup can produce an estimated vertical force of 140 N [31].
- Two DC motors: one motor to drive the mobile actuator along the links, and the other motor to rotate the joints of the links. Both motors are 12 mm in diameter (6-9 Volts manufactured by Pololu), which can be purchased at different gear ratios and can be fitted with magnetic encoders.
- An off-the shelf servo motor to actuate the gripper.

Control

The robot is controlled by two electronic control boards that are synchronized using RF module communication. The mobile actuator is controlled with a Teensy 3.5 controller (compatible with Arduino software) that controls its locomotion, its rotational mechanism and its gripper. The angular displacement of the rotational mechanism is measured using a magnetic encoder fitted to the motor's shaft and yields 12 counts per motor revolution. The motors are powered by two 3.7 Volts 800 mAh LiPo batteries connected in series.

To ensure that the mobile actuator stops accurately at the precise location to engage the gears of the links and rotate the joints, tiny magnets were inserted in the centers of the joints and a magnetic Hall effect sensor (A1302) was attached to the mobile actuator. The stepper motor that actuates the vertical motion is controlled with an Arduino Uno board. The two controllers communicate via a NRF24L01 Radio Transceiver Module that transmits and receives commands and other data such as location and orientation between the two controllers.

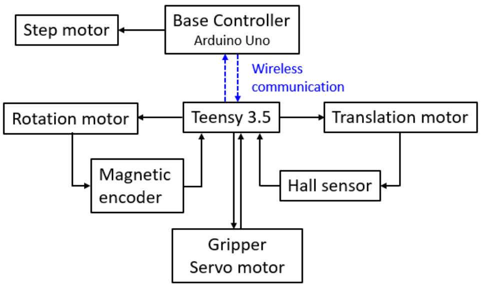

Figure 6. The electronic control system of the robot.

KINEMATIC MODEL

We assume that our robot is composed of N identical links (not including the base link) whose length is L, connected using N rotational joints. Since the manipulator is confined to the horizontal plane (x,y) and the linear screw to the vertical direction (z), the motion of the two mechanisms can be decoupled and the analysis can be performed separately.

Position and Speed

The links are numbered from 0 (the base link) to N which represents the last link in the serial arm. The joint angle j between the links j-1 and j is denoted by θ_j, and the relative orientation of link j to the base link by α_j. The position of joint j (x_j, y_j, z) of the robot and its orientation α_j are given by:

$$\mathbf{X_j} = \begin{bmatrix} x_j \\ y_j \\ z \\ \alpha_j \end{bmatrix} = \begin{bmatrix} L\sum_{m=1}^{j}\cos\left(\sum_{m=1}^{n}\theta_m\right) \\ L\sum_{n=1}^{j}\sin\left(\sum_{m=1}^{n}\theta_m\right) \\ z_j \\ \sum_{m=1}^{j}\theta_m \end{bmatrix} \quad (1).$$

The mobile actuator in our robot can either travel along the links or rotate the joints. Therefore, the speed $\dot{\mathbf{X}}_\mathbf{j}$ of a joint j can be calculated using the Jacobian matrix $\mathbf{J_j}$ like other regular serial robots:

$$\dot{\mathbf{X}}_\mathbf{j} = \mathbf{J_j}\begin{bmatrix} \dot{\boldsymbol{\theta}} \\ \dot{z} \end{bmatrix} \quad (2).$$

where the Jacobian matrix is defined as:

$$\mathbf{J_j} = \begin{bmatrix} \frac{\partial X}{\partial \theta_1} \cdots \frac{\partial X}{\partial \theta_j}, \frac{\partial X}{\partial z} \end{bmatrix} \quad (3).$$

Note that since a single mobile actuator is currently being used, the different joints of the serial arm can be actuated one at a time. The total time required to reconfigure the angles of the joints and reach a specific target is composed of the time required to travel along the links, to engage the joints, rotate them and disengage from them. The vertical motion along the vertical direction can be performed in parallel to the motion of the serial arm.

If we assume a constant lifting and lowering velocity V_z of the vertical motor and constant linear and rotational speeds of the mobile actuator, respectively V_m and ω, the time required to reach a target is:

$$\Delta T = \mathrm{Max}\left(\frac{1}{\omega}\sum_{1}^{N}\left|\Delta\theta_j\right| + \frac{d_T}{V_m} + n\cdot T_{\mathrm{STOP}}; \frac{\Delta z}{V_z}\right) \qquad (4)$$

where $\Delta\theta_j$ the is rotation of joint j, d_T is the total distance travelled by the mobile actuator, n is the number of rotated joints and T_{STOP} is the time required to start and stop the mobile actuator.

Workspace

Given that the joints in the current design are limited to rotating by a maximum of 45 degrees to either side, we determined the work volume of the serial arm in the 2D space as a function of the number of links. The work volume was determined by exhaustively searching the total space for possible solutions (not including orientation), using the motion planning algorithm presented in Section IV. At six links, the arm can already reach areas behind its base. The size of the work area (2D space) continues to increase with the number of links. The size of the workspace is nearly four times larger with 10 links compared to its size with 6 links. The size of the workspace as a function of the links is presented in 0

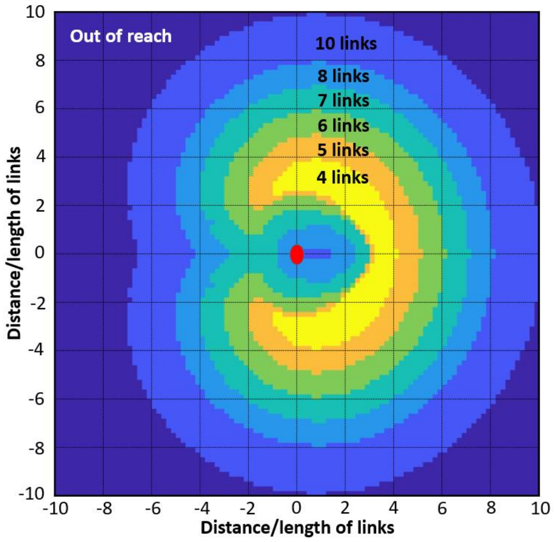

Figure 7. Top view of the work volume of the robot as a function of the number of links.

SIZE OF THE WORKSPACE AS A FUNCTION OF *N*.

. of links N	4	5	6	7	8	10
Work space [L^2]	8.3	18.9	35.8	58.7	83.5	136.7

where L is the length of a single link.

2D MOTION PLANNING ALGORITHM

The MASR robot is a minimally actuated overly redundant robot; i.e., there is an infinite number of solutions to reach a specific point in the plane using the robotic arm. Our aim in this planning algorithm is to reduce the location error, the travelling distance of the mobile actuator, its number of stops to rotate the joints and the total time required to perform a task. Assuming an obstacle-free space, and that the arm's initial configuration is $\boldsymbol{\theta}\mathbf{i}$, (initial position and orientation $\mathbf{Xi}=(x_i,y_i,\alpha_i)$), the goal is to determine the joint rotation $\Delta\boldsymbol{\theta}_\mathbf{j}$ which will lead the arm to the final location $\mathbf{Xf}=(x_f,y_f,\alpha_f)$.

Our algorithm is based on minimizing a cost function F($\Delta\boldsymbol{\theta}_\mathbf{j}$, $\boldsymbol{\theta}\mathbf{i}$, $\mathbf{X}_\mathbf{f}$) which combines the original orientation of the links, the proximity of the robot to the target point and the variation of the joint angles from the original to the final configuration. We minimized the function using Matlab's *fmincon* function which can find a *local minimum* within given upper and lower bounds (such as the minimum and maximum values of the rotation angle, negative 45 degrees to positive 45 degrees). To increase its chances of finding the global minimum and improve the results, we ran the function 100 times with different randomly chosen original solution guesses and the solution with the lowest cost function was chosen. Throughout this analysis, we assumed that the robot was composed of 10 identical links whose length L is 5 cm (similar to the experimental robot). In the following examples, solutions were accepted only if the maximum distance from the target was less than 0.2 cm and the orientation error of the last link was less than 0.5 degrees.

*Reaching a Target with the Tip of the Last Link (**LL**)*

Although the mobile actuator carries the gripper, in many applications grasping an object may be possible only if the gripper is located on the last link of the serial arm. In this case, the tip of the robot must reach the desired location and the last link must have the same orientation as the target. The cost function F is composed of the three functions, f_{TIP} and f_{OR} which respectively weigh the distance and orientation of the last link from the target and the function f_{STOPS} which weighs the number of the actuated joints.

$$F\left(\boldsymbol{\Delta\theta}_\mathbf{j}, \boldsymbol{\theta}_\mathbf{i}, \mathbf{X}_\mathbf{f}\right) = w_1 f_{\mathrm{TIP}} + w_2 f_{\mathrm{OR}} + w_3 f_{\mathrm{STOPS}} \qquad (5).$$

The proximity function f_{TIP} is simply defined as the norm of the vector error of the tip of the robot from the target point:

$$f_{\mathrm{TIP}} = \mathrm{norm}\left(\mathbf{X}_\mathbf{F} - \mathbf{X}_\mathbf{N}\right) \qquad (6).$$

The orientation function f_{OR} is the square of the difference between the orientation of the last joint to the orientation of the tip of the robot:

$$f_{\mathrm{OR}} = \left(\alpha_N - \alpha_T\right)^2 \qquad (7).$$

The function f_{STOPS} is negative and sums the values of the changes in the joints at the power n.

$$f_{\mathrm{STOPS}} = -\sum_{j=1}^{N}\left|\Delta\theta_j^n\right| \qquad (8).$$

If the power n is larger than 1, the algorithm attempts to increase the variation of the joints. Given that the sum of the variation is limited by the orientation of the last link, the algorithm attempts to reduce the number of active joints and increase their rotation. In the solution we used identical weights w_1=w_3=1 whereas w_2=200 in order to increase its influence. The value of $w_2 * f_{\mathrm{OR}}$ is equal to one if the error is nearly 0.2 degrees (0.0035 Radians).

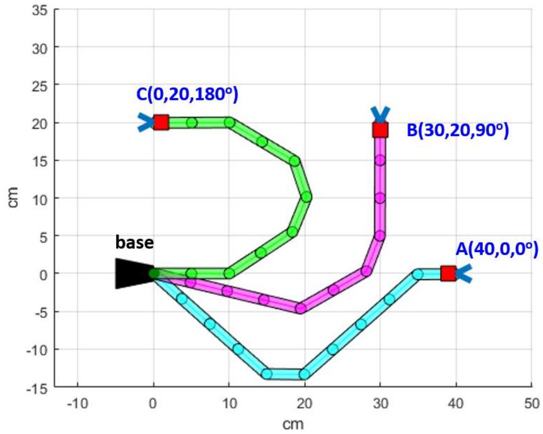

Figure 8. Starting from an initial configuration where all the joints were at 0 degrees, the robot reaches points A, B, and C using the LL method.

SOLUTION FOR A,B, AND C USING THE "LL" METHOD.

nt No.	Initial config.	Point A (40,0,0º)	Point B (30,20,90º)	Point C (0,20,180º)
1	0	-41.8	-13.4	0
2	0	0	0	0
3	0	0	0	33.2
4	0	0	0	0
5	0	0	43	34.1
6	0	41.6	0	40.7
7	0	42	39.2	40.7
8	0	0	20.9	0
9	0	0	0	31.1
10	0	-41.4	0	0
Active joints	-	4	4	5
Δd [cm]	-	0.07	0.13	0.07
Δθ [deg]	-	-0.29	0.07	0.38
Travelled d.	-	50 cm	50 cm	50 cm
rotation		167º	117º	180 º
Conv. rate		69%	75%	84%

In the following example (Figure 8), we searched for a solution to three different target points with given orientations $\mathbf{X_A}$(40,0,0º), $\mathbf{X_B}$(30,20,90º), and $\mathbf{X_C}$(0,20,180º). Starting from an initial configuration where the mobile actuator was at the origin and all the joint angles were 0º, the algorithm success rate in finding a solution within the accepted range (position error < 0.2 cm and orientation error < 0.5 degrees) was 69% in A, 75% in B, and 84% in C. For point A, a solution was found by rotating only four joints and the errors were 0.07 cm and -0.29 degrees. In B, a solution was found by rotating only four joints and the error is 0.13 cm and 0.07 degrees. In C, five joints were rotated, and the error was 0.07 cm and 0.38 degrees. For each point, one of the results with the smallest number of actuated joints is presented in 0The average success rate of the algorithm in finding a solution in the whole workspace for 10 links which includes 3342 points (as per Figure 7) is 92.4 % while the average running time per solution is 1.5 seconds. Note that the algorithm does not account for self-collisions. However, a self-collision is extremely unlikely because the joints are limited to rotate in the range of ±45 degrees only and that the function f_{STOPS} attempts to reduce the number of joint rotation.

*Reaching a Target with Any Link (**AL**)*

One of the unique features of the MASR robot is that its gripper can reach a specific target if any of the links is above or below the target (see

Figure 10 and video). This feature is especially useful if the target point is close to the base link or if the mobile actuator is required to move objects along the path of the links. If the target point is above or below a given link j, the distance from the line along (collinear) the link j to the target, denoted by d_{LINK}, must be zero. The target point must also be within the boundaries of the link; i.e., between joint j and j+1 (see Figure 9). We denote the distance between the target to adjacent joints by d_j and d_{j+1}. In order to satisfy this condition, both distances must be simultaneously smaller than the length of the link L.

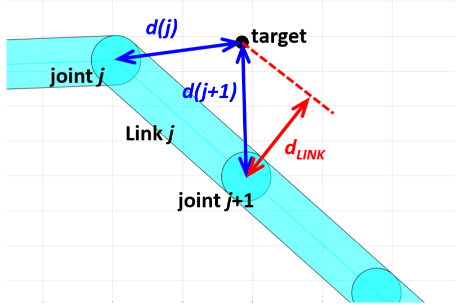

Figure 9. The distance of the target from link j and the adjacent joints (j and j+1).

The cost function in the *AL* case is defined as:

$$F\left(\Delta\boldsymbol{\theta}_j,\boldsymbol{\theta}_i,\mathbf{X}_f\right)=w_1 f_{\mathrm{LINK}}+w_2 f_{\mathrm{OR}}+w_3 f_{\mathrm{STOPS}} \qquad (9).$$

where f_{OR} and f_{STOPS} and the weights w_i are identical to the *LL* case, and f_{LINK} is defined as:

$$f_{\mathrm{LINK}}=d_{\mathrm{LINK}}{}^2+f_{\mathrm{JOINT}}\left(j\right)+f_{\mathrm{JOINT}}\left(j+1\right) \qquad (10)$$

and the function f_{JOINT} is:

$$f_{\mathrm{JOINT}}\left(j\right)=\mathrm{abs}\left(L-d\left(j\right)\right)-\left(L-d\left(j\right)\right) \qquad (11).$$

The cost function $f_{\mathrm{JOINT}}(j)$ becomes zero if the distance between the joint to the target point is less than L and positive (linearly monotonous) if the distance is larger than L. Minimizing the combination of $f_{\mathrm{JOINT}}(j)$, $f_{\mathrm{JOINT}}(j+1)$, together with the distance d_{LINK} ensures that the target point is on the link j.

The results of the algorithm that found an optimal solution for the three points A,B and C (points identical to the previous section), are presented in

Figure 10 and summarized in 0The algorithm successfully found solutions at high convergence rates (respectively 96%, 84% and 98% for A, B and C). The solution for A is trivial and the mobile actuator travelled a distance of 40 cm along the links without rotating any joint. In B, the mobile actuator rotated only 3 joints and reached the point using its 9$^{\text{th}}$ link after travelling 45 cm. In C, the rotation of 5 joints was required and the robot reached the point with its 6$^{\text{th}}$ link.

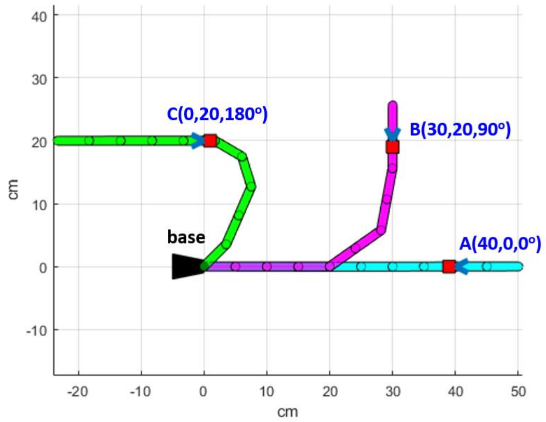

Figure 10. Starting at an initial configuration where all the joints were at 0 degrees, the robot reached points A, B, and C using the AL method.

SOLUTION FOR A, B, AND C USING THE "AL" METHOD.

nt No.	Initial config.	Point A (40,0,0º)	Point B (30,20,90º)	Point C (0,20,180º)
1	0	0.0	0.0	45.0
2	0	0.0	0.0	21.5
3	0	0.0	0.0	0
4	0	0.0	0.0	40.7
5	0	0.0	35.2	42.4
6	0	0.0	0.0	30.4
7	0	0.0	44.2	0
8	0	0.0	0.0	0
9	0	0.0	10.2	0
10	0	0.0	0.0	0
Active joints	-	0	3	5
Δd [cm]	-	0.00	0.004	0.006
Δθ [deg]	-	0.00	0.23	0.03
Travelled d.	-	40 cm	45 cm	30 cm
Rotation		0º	90º	180º
Conv. Rate		96%	84%	98%

Comparing the LL and the AL Methods

In the previous section, the robot travelled from its original location (straight line where the mobile actuator was located at the origin O) to points A, B and C. In this section, we compare the distance travelled by the mobile actuator, the total angular rotation of the joints, the number of stops and the total time. Using Eq. (4) and assuming that V_m =20 cm/s and ω=360 degrees/s and that T_{STOP}=0.1 s, the total time required for performing the mission can be calculated. A comparison between the two methods is presented in 0The results show that the AL method is substantially faster than LL (by 20% to 45%).

Next, we compared the two methods when performing consecutive tasks by travelling to the origin O and then to points A, B and C. The results of the comparison are presented in Figure 11 and table V.

COMPARING THE METHODS REACHING POINTS A, B AND C

	Point A	Point B	Point C
stance LL	45	45	45
stance AL	40	45	25
gular LL [deg.]	167	116	180
gular AL [deg.]	0	90	180
ps LL	5	6	7
ps AL	1	3	5
tal time LL [s]	3.7	3.5	4
tal time AL [s]	2.1	3	2.7

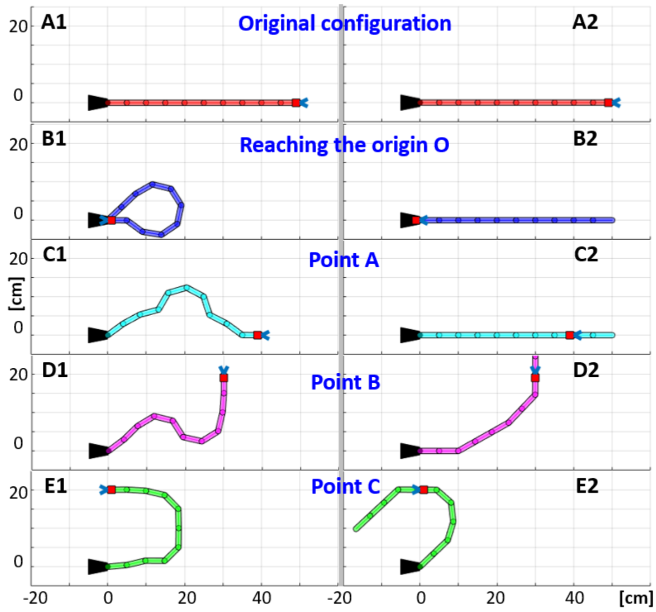

Figure 11. Comparison of the LL and AL methods performing consecutive tasks. Starting from its original configuration, the robot moves its mobile actuator to points O, A, B and C.

COMPARING THE METHODS WHEN TRAVELLING ALONG THE PATH OABC

	O	OA	AB	BC	OABC
stance LL [cm]	45	90	90	90	315
stance AL [cm]	)	40	45	75	160
gular LL [º]	339	209	333	266	1147
gular AL[º]	0	0	90	133	223
ps LL	8	5	7	7	27
ps AL	0	1	4	5	10
tal time AL [s]	4.9	6.2	7.1	6.7	24.8
tal time L[s]	0	2.1	3.1	5	10.3

Starting from the original configuration "A1", the robot in the LL case must rotate 9 of its joints to reach the origin "B1", whereas in the AL method it does not rotate any joints at all "B2". The same holds in case "C" as in the AL method, where the mobile actuator only needs to travel to link 8 without rotating any of its joints. In case "D2", using the AL method, the target can be reached by only using 9 links and in "E2" by only using 6 links. 0presents the number of steps required and time elapsed for task performance. It shows that performing the task using the AL method is substantially faster (nearly 60%) and reduces the distance travelled by the mobile actuator and rotated joints.

EXPERIMENTS AND RESULTS

This section presents the results of the experiments conducted with a 3D printed prototype of the robot. We tested its full functionality in multiple experiments which included reaching different points in 3D space, picking up objects with the mobile actuator, translating them using the mobile actuator while travelling over the links and releasing them at the target points. The experiments were pre-planned offline using our optimization algorithm and performed automatically using the robot (see video).

Translating an Object Located Above the Links

The first experiment using this robot mimicked picking a piece of fruit from a tree and placing it in a basket. Starting at A, the vertical actuator raises the arm by 26 cm while the mobile actuator advances slightly towards the ball "B" hanging from the top with a nylon wire. The mobile actuator grasps the ball in “C” and advances to the 5th joint while rotating it by 4 degrees “D”. Then, the mobile actuator advances to the 6th joint while rotating it by 24 degrees “E” and continues towards the 10th link to drop the ball into the target bowl “F”. See attached video.

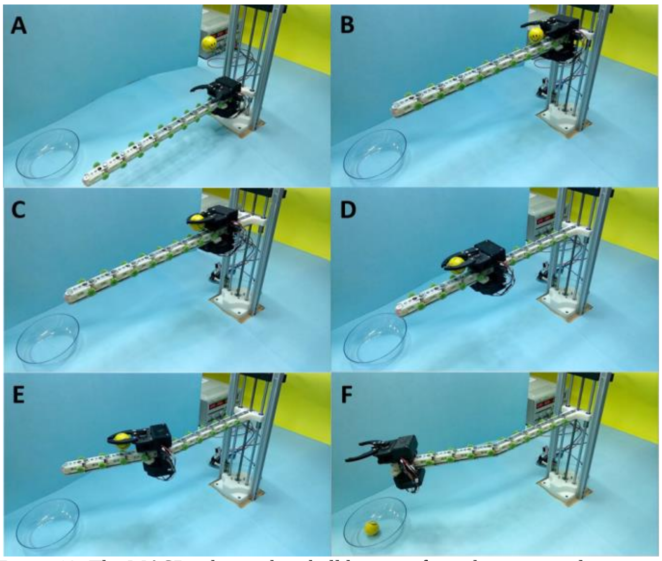

Figure 12. The MASR robot picks a ball hanging from the top, translates it along the links and drops it into a basket.

Relocating an Object

In this experiment, the robot’s task was to move the position of a cup using a minimal number of joints. The origin and target locations of the cup were at different heights. Starting in “A”, the linear vertical actuator raises the arm by 10 cm. Moving forward, the mobile actuator advances to the 7th and the 8th joints and rotates their angles by 28 and 16 degrees respectively “B”. Then, the mobile actuator continues advancing along the links to reach cup “C”. After grasping the cup, the linear vertical actuator raises the arm by 12 cm, while the mobile actuator returns to the 8th link “D” and rotates it into negative 16 degrees and the 7th link into negative 28 degrees “E”. The mobile actuator then moves along the links and places the cup in the target location “F”. See attached video.

Reaching Around an Obstacle

In the last experiment presented here, the mobile actuator rotated the links to go around an obstacle (simulating a wall) to reach the target. The wall was 7 cm away in the *y* direction from the origin of the robot and was 25 cm long (from x= 0 to x=25 cm). The target location was (10, -20). Starting from straight configuration “A”, the mobile actuator travels toward the 8th joint (“B” to “D”) and rotates the joints [(5, -38 º) (6, -39 º) (7, -38 º) (8, -35 º)] as it advances. Then the mobile actuator proceeds to the last link “E” and releases the ball “F”. See attached video.

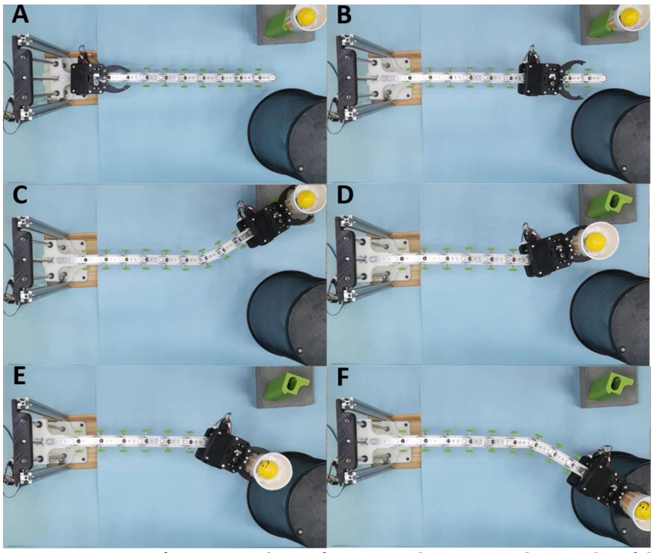

Figure 13. Starting from a straight configuration, the MASR relocates the of the cup.

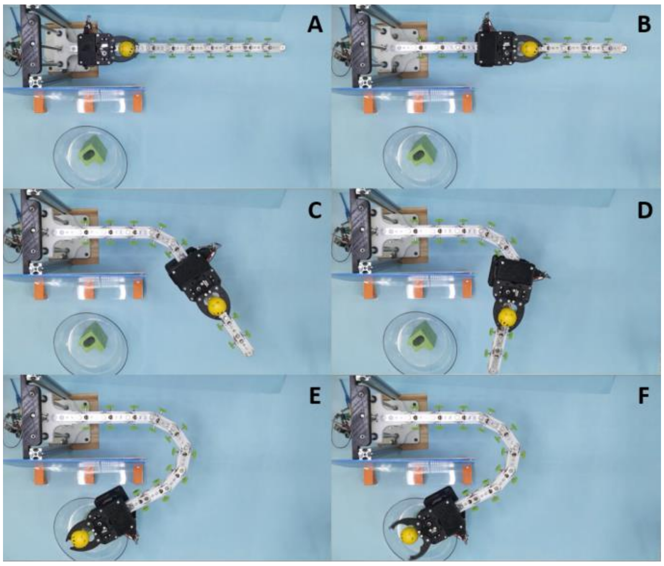

Figure 14. Starting from straight configuration, the MASR rotates its links to turn around an obstacle.

CONCLUSIONS

In this paper, we presented a novel serial robot composed of a multi linkage arm with passive joints and a mobile actuator that can travel along the arm and rotate the links. The mobile actuator is fitted with a gripper that allows it to grasp objects along its path and translate them quickly along the arm. This design makes it possible to reduce the size of the robot, its weight and simplify its design. As it has no wiring along the links, the links can be easily replaced and their size and number simply changed according to the requirement of the task. The mobile actuator can also be replaced, and more than one mobile actuator can be used.

We developed a locomotion algorithm based on optimizing a time-based function to minimize the operation time and actuation of the robot. Since our gripper can be moved along the links, we compared the time requirements for a task in which the robot relocates an object from one point to another with a given orientation for two situations: 1) the gripper can only grasp an object when the gripper is at the last link “LL”. 2) The gripper can grasp objects at any link along the arm

"AL". A comparison of the time elapsed in each of the two methods shows that in the second case, the time can be reduced by nearly three-fold.

Finally, we developed an experimental prototype of the robot which can automatically perform its pre-planned tasks. We used the robot to demonstrate multiple tasks which include relocating objects by rotating a minimal number of joints and translating objects along the robot's arm. The 3D printed version with aluminum reinforcement is designed for a workload 0.5 kg which can cause a deformation of up to 0.5 cm at its tip due to the flexibility of the links and the backlash of the joints. Decreasing the number of links will decrease the deformation and vice versa.

Note that while this robot is very simple and lightweight, it is substantially slower than regular fully actuated serial arms. Therefore, this robot should be used in applications where high speed is not required such as space applications, agriculture, maintenance, painting and search and rescue operations, for example.

Our future work will focus on using multiple mobile actuator, improving the design and developing a metal version to reduce the deformation. We also plan to study the mobility of the MASR in 3D space and developing more advanced motion planning algorithms.

ACKNOWLEDGEMENTS

This research was supported in part by the Israel Ministry of Science and Technology and by the Pearlstone center for Aeronautical Studies.

REFERENCES

[1] K. Ning, and F. WÖrgÖtter, "A Novel Concept for Building a Hyper-Redundant Chain Robot," *IEEE Transactions on Robotics*, vol. 25, no. 6, pp. 1237-1248, 2009.

[2] P. Schrock, F. Farelo, R. Alqasemi, and R. Dubey, "Design, simulation and testing of a new modular wheelchair mounted robotic arm to perform activities of daily living," IEEE International Conference on Rehabilitation Robotics, Kyoto, pp. 518-523, 2009.

[3] E. Shammas, A. Wolf, H. B. Brown, and H. Choset, "New joint design for three-dimensional hyper redundant robots," IEEE/RSJ International Conference on Intelligent Robots and Systems, Las Vegas, NV, USA, vol. 3, pp. 3594-3599, 2003.

[4] A. Wolf, H. B. Brown, R. Casciola, A. Costa, M. Schwerin, E. Shamas, and H. Choset , "A mobile hyper redundant mechanism for search and rescue tasks," IEEE/RSJ International Conference on Intelligent Robots and Systems, Las Vegas, NV, USA, vol. 3, pp. 2889-2895, 2003.

[5] I. Erkmen, A. M. Erkmen, F. Matsuno, R. Chatterjee, and T. Kamegawa, "Snake robots to the rescue!" *IEEE Robotics & Automation Magazine*, vol. 9, no. 3, pp. 17-25, 2002.

[6] H. Maruyama, and K. Ito, "Semi-autonomous snake-like robot for search and rescue," IEEE Safety Security and Rescue Robotics, Bremen, pp. 1-6, 2010.

[7] T. Kamegawa, T. Yarnasaki, H. Igarashi, and F. Matsuno, "Development of the snake-like rescue robot "kohga"," IEEE International Conference on Robotics and Automation, New Orleans, LA, USA, vol. 5, pp. 5081-5086, 2004.

[8] J. Borenstein, M. Hansen, and A. Borrell, "The OmniTread OT-4 Serpentine Robot 1 – Design and Performance," *Journal of Field Robotics*, vol. 24, pp. 601-621, 2007.

[9] M. Arai, Y. Tanaka, S. Hirose, H. Kuwahara, and S. Tsukui, "Development of "Souryu-IV" and "Souryu-V": Serially connected crawler vehicles for in-rubble searching operations," *Journal of Field Robotics*, vol. 25, pp. 31-65, 2008.

[10] K. Suzuki, A. Nakano, G. Endo, and S. Hirose, "Development of multi-wheeled snake-like rescue robots with active elastic trunk," IEEE/RSJ International Conference on Intelligent Robots and Systems, Vilamoura, pp. 4602-4607, 2012.

[11] H. Komura, H. Yamada, and S. Hirose, "Development of snake-like robot ACM-R8 with large and mono-tread wheel," *Advanced Robotics*, vol. 29, pp. 1081-1091, 2015.

[12] K. Ito, and M. Haruo. "Semi-autonomous serially connected multi-crawler robot for search and rescue," *Advanced Robotics*, vol. 30, no. 7, pp. 489-503, 2016.

[13] T. Ota, A. Degani, D. Schwartzman, B. Zubiate, J. McGarvey, H. Choset and M. A. Zenati, "A Highly Articulated Robotic Surgical System for Minimally Invasive Surgery," The Annals of Thoracic Surgery, vol. 87, pp. 1253-1256, 2009.

[14] A. Degani, H. Choset, A. Wolf and M. A. Zenati, "Highly articulated robotic probe for minimally invasive surgery," IEEE International Conference on Robotics and Automation, Orlando, FL, pp. 4167-4172, 2006.

[15] K. Ikuta, T. Hasegawa and S. Daifu, "Hyper redundant miniature manipulator "Hyper Finger" for remote minimally invasive surgery in deep area," IEEE International Conference on Robotics and Automation, Taipei, Taiwan, vol. 1, pp. 1098-1102, 2003.

[16] N. Simaan, R. Taylor and P. Flint, "A dexterous system for laryngeal surgery," IEEE International Conference on Robotics and Automation, New Orleans, LA, USA, vol. 1, pp. 351-357, 2004.

[17] J. Burgner-Kahrs, D. C. Rucker and H. Choset, "Continuum Robots for Medical Applications: A Survey," IEEE Transactions on Robotics, vol. 31, no. 6, pp. 1261-1280, 2015.

[18] R. J. Webster, A. M. Okamura and N. J. Cowan, "Toward Active Cannulas: Miniature Snake-Like Surgical Robots," IEEE/RSJ International Conference on Intelligent Robots and Systems, Beijing, pp. 2857-2863, 2006.

[19] Z. Mu, T. Liu, W. Xu, Y. Lou, and B. Liang, "Dynamic feedforward control of spatial cable-driven hyper-redundant manipulators for on-orbit servicing," *Robotica*, vol. 37, no. 1, pp. 18–38, 2019.

[20] V. A. Sujan, M. D. Lichter, and S. Dubowsky, "Lightweight hyper-redundant binary elements for planetary exploration robots," IEEE/ASME International Conference on Advanced Intelligent Mechatronics, Como, Italy, vol. 2, pp. 1273-1278, 2001.

[21] M. Yim, K. Roufas, D. Duff, Y. Zhang, C. Eldershaw, and S. Homans, "Modular Reconfigurable Robots in Space Applications," *Autonomous Robots*, vol. 14, pp. 225–237, 2003.

[22] C. Fan, Y. Zhang, Z. Xie, Y. Liu, Z. Li, C. Li, and H. Liu, "Design of Space Robotic Arm-Hand System and Operation Research," IEEE International Conference on Mechatronics and Automation, Changchun, pp. 481-486, 2018.

[23] I. D. Walker, "Robot strings: Long, thin continuum robots," IEEE Aerospace Conference, Big Sky, MT, USA, pp. 1-12, 2013.

[24] L. Pfotzer, S. Klemm, A. Rönnau, J. M. Zöllner, and R. Dillmann, "Autonomous navigation for reconfigurable snake-like robots in challenging, unknown environments," *Robotics and Autonomous Systems*, vol. 89, pp. 123-135, 2017.

[25] M. S. Menon, V. C. Ravi, and A. Ghosal, "Trajectory Planning and Obstacle Avoidance for Hyper-Redundant Serial Robots," *ASME. J. Mechanisms Robotics*, vol. 9, no. 041010-1, 2017.

[26] E. K. Xidias, "Time-optimal trajectory planning for hyper-redundant manipulators in 3D workspaces," *Robotics and Computer-Integrated Manufacturing*, vol. 50, pp. 286-298, 2018.

[27] J. Zhao, L. Zhao, and Y. Wang, "A Novel Method for the Motion Planning of Hyper-redundant Manipulators Based on Monte Carlo," *Mechanism and Machine Science*, vol. 408, pp. 11-22, 2017.

[28] A. Motahari, H. Zohoor, and M. H. Korayem, "A new motion planning method for discretely actuated hyper-redundant manipulators," *Robotica*, vol. 35, no. 1, pp. 101–118, 2017.

[29] M. P. Mann, L. Damti, G. Tirosh, and D. Zarrouk, "Minimally actuated serial robot", *Robotica*, vol. 36, no. 3, pp. 408–426, 2018.

[30] T. Kislassi, and D. Zarrouk, "A Minimally Actuated Reconfigurable

Continuous Track Robot," *IEEE Robotics and Automation Letters*, doi: 10.1109/LRA.2019.2959237, 2019.

[31] R. L Norton, "Machine design, an integrated approach", (Pearson, Edition 5), 2013.

References

[32] M. P. Mann, L. Damti, G. Tirosh, and D. Zarrouk, “Minimally actuated serial robot”, *Robotica*, vol. 36, no. 3, pp. 408–426, 2018.

[33] T. Kislassi, and D. Zarrouk, “A Minimally Actuated Reconfigurable Continuous Track Robot,” IEEE Robotics and Automation Letters, doi: 10.1109/LRA.2019.2959237, 2019.

[34] T. Fong and I. Nourbakhsh, “Peer-to-Peer Human-Robot Interaction for Space Exploration,” AAAI Fall Symposium - Technical Report, 2004.

[35] J. J. Marquez, “Unique considerations for human-robotic interaction in human spaceflight,” NASA Ames Research Center, 2017.

[36] M. Hiltz, C. Rice and K. Boyle, “Canadarm: 20 Years of Mission Success through Adaptation,” International Symposium on Artificial Intelligence and Robotics & Automation in Space, Quebec:CSA, 2001.

[37] D. A. Whelan, E. A. Adler, S. B. Wilson and G. M. Roesler, “DARPA Orbital Express program: Effecting a revolution in space-based systems,” SPIE - The International Society for Optical Engineering, 10.1117/12.406656, 2000.

[38] M. Oda, “Space robot experiments on NASDA's ETS-VII satellite-preliminary overview of the experiment results,” IEEE International Conference on Robotics and Automation, USA, vol. 2, pp. 1390-1395, 1999.

[39] C. Fan, Y. Zhang, Z. Xie, Y. Liu, Z. Li, C. Li, and H. Liu, “Design of Space Robotic Arm-Hand System and Operation Research,” IEEE International Conference on Mechatronics and Automation, Changchun, pp. 481-486, 2018.

[40] L.W. Tsai, “Robot analysis: The mechanics of serial and parallel manipulators”,

Engineering & Materials Science, Wiley-Interscience, 1st edition, 1999.

[41] "KUKA Robotics Corporation". [Online]. http://www.kuka-robotics.com/en/

[42] "ABB Technologies Ltd.", 12 2016. [Online]. http://new.abb.com/products/robotics

[43] J. Ostrowski and J. Burdick, “Gait kinematics for a Serpentine Robot”, the International Conference on Robotics and Automation, 1996.

[44] J. W. Burdick, J. Radford and G. S. Chirikjian, “Sidewinging Locomotion Gait for Hyper redundant robots”, *Advanced robotics*, vol. 9, no. 3, pp 195-216, 1995.

[45] G. S. Chirikjian and J. W. Burdick, "A hyper-redundant manipulator," *IEEE Robotics & Automation Magazine*, vol. 1, no. 4, pp. 22-29, Dec. 1994.

[46] P. Liljeback, K. Pettersen, O. Stavdahl and J. Gravdahl, “A review on modelling, implementation, and control of snake robots”, *Robotics and Autonomous Systems*, vol. 60, pp. 29-40, 2012.

[47] P. Liljeback, K. Pettersen, O. Stavdahl and J. Gravdahl, “Snake Robots - Modelling, Mechatronics, and Control”, Springer, 2013.

[48] K. Ning, and F. WÖrgÖtter, “A Novel Concept for Building a Hyper-Redundant Chain Robot,” *IEEE Transactions on Robotics*, vol. 25, no. 6, pp. 1237-1248, 2009.

[49] P. Schrock, F. Farelo, R. Alqasemi, and R. Dubey, “Design, simulation and testing of a new modular wheelchair mounted robotic arm to perform activities of daily living,” IEEE International Conference on Rehabilitation Robotics, Kyoto, pp. 518-523, 2009.

[50] E. Shammas, A. Wolf, H. B. Brown, and H. Choset, “New joint design for three-dimensional hyper redundant robots,” IEEE/RSJ International Conference on Intelligent

Robots and Systems, Las Vegas, NV, USA, vol. 3, pp. 3594-3599, 2003.

[51] V. V. Anderson, R. C. Horn, “Tensor-arm Manipulator design,” ASME Trans., vol. 67, pp. 1-12, 1967.

[52] A. Wolf, H. B. Brown, R. Casciola, A. Costa, M. Schwerin, E. Shamas, and H. Choset , “A mobile hyper redundant mechanism for search and rescue tasks,” IEEE/RSJ International Conference on Intelligent Robots and Systems, Las Vegas, NV, USA, vol. 3, pp. 2889-2895, 2003.

[53] I. Erkmen, A. M. Erkmen, F. Matsuno, R. Chatterjee, and T. Kamegawa, “Snake robots to the rescue!” *IEEE Robotics & Automation Magazine*, vol. 9, no. 3, pp. 17-25, 2002.

[54] H. Maruyama, and K. Ito, “Semi-autonomous snake-like robot for search and rescue,” IEEE Safety Security and Rescue Robotics, Bremen, pp. 1-6, 2010.

[55] T. Kamegawa, T. Yarnasaki, H. Igarashi, and F. Matsuno, “Development of the snake-like rescue robot “kohga”,” IEEE International Conference on Robotics and Automation, New Orleans, LA, USA, vol. 5, pp. 5081-5086, 2004.

[56] J. Borenstein, M. Hansen, and A. Borrell, “The OmniTread OT-4 Serpentine Robot 1 – Design and Performance,” *Journal of Field Robotics*, vol. 24, pp. 601-621, 2007.

[57] M. Arai, Y. Tanaka, S. Hirose, H. Kuwahara, and S. Tsukui, “Development of “Souryu-IV” and “Souryu-V”: Serially connected crawler vehicles for in-rubble searching operations,” *Journal of Field Robotics*, vol. 25, pp. 31-65, 2008.

[58] K. Suzuki, A. Nakano, G. Endo, and S. Hirose, “Development of multi-wheeled snake-like rescue robots with active elastic trunk,” IEEE/RSJ International Conference on Intelligent Robots and Systems, Vilamoura, pp. 4602-4607, 2012.

[59] H. Komura, H. Yamada, and S. Hirose, “Development of snake-like robot ACM-R8 with large and mono-tread wheel,” *Advanced Robotics,* vol. 29, pp. 1081-1091, 2015.

[60] K. Ito, and M. Haruo. “Semi-autonomous serially connected multi-crawler robot for search and rescue,” *Advanced Robotics,* vol. 30, no. 7, pp. 489-503, 2016.

[61] T. Ota, A. Degani, D. Schwartzman, B. Zubiate, J. McGarvey, H. Choset and M. A. Zenati, “A Highly Articulated Robotic Surgical System for Minimally Invasive Surgery,” The Annals of Thoracic Surgery, vol. 87, pp. 1253-1256, 2009.

[62] A. Degani, H. Choset, A. Wolf and M. A. Zenati, “Highly articulated robotic probe for minimally invasive surgery,” IEEE International Conference on Robotics and Automation, Orlando, FL, pp. 4167-4172, 2006.

[63] K. Ikuta, T. Hasegawa and S. Daifu, “Hyper redundant miniature manipulator “Hyper Finger” for remote minimally invasive surgery in deep area,” IEEE International Conference on Robotics and Automation, Taipei, Taiwan, vol. 1, pp. 1098-1102, 2003.

[64] N. Simaan, R. Taylor and P. Flint, “A dexterous system for laryngeal surgery,” IEEE International Conference on Robotics and Automation, New Orleans, LA, USA, vol. 1, pp. 351-357, 2004.

[65] J. Burgner-Kahrs, D. C. Rucker and H. Choset, “Continuum Robots for Medical Applications: A Survey,” *IEEE Transactions on Robotics,* vol. 31, no. 6, pp. 1261-1280, 2015.

[66] R. J. Webster, A. M. Okamura and N. J. Cowan, “Toward Active Cannulas: Miniature Snake-Like Surgical Robots,” IEEE/RSJ International Conference on Intelligent Robots and Systems, Beijing, pp. 2857-2863, 2006.

[67] Z. Mu, T. Liu, W. Xu, Y. Lou, and B. Liang, “Dynamic feedforward control of spatial cable-driven hyper-redundant manipulators for on-orbit servicing,” *Robotica,* vol.

37, no. 1, pp. 18–38, 2019.

[68] V. A. Sujan, M. D. Lichter, and S. Dubowsky, “Lightweight hyper-redundant binary elements for planetary exploration robots,” IEEE/ASME International Conference on Advanced Intelligent Mechatronics, Como, Italy, vol. 2, pp. 1273-1278, 2001.

[69] M. Yim, K. Roufas, D. Duff, Y. Zhang, C. Eldershaw, and S. Homans, “Modular Reconfigurable Robots in Space Applications,” *Autonomous Robots*, vol. 14, pp. 225–237, 2003.

[70] I. D. Walker, “Robot strings: Long, thin continuum robots,” IEEE Aerospace Conference, Big Sky, MT, USA, pp. 1-12, 2013.

[71] P. Singh and C. Krishna, “Continuum Arm Robotic Manipulator: A Review,” *Universal Journal of Mechanical Engineerings*, vol. 2, no. 6, pp. 193-198, 2014.

[72] H. Choset, K. Lynch, S. Hutchinson, G. Kantor, W. Burgard, L. Kavraki and S. Thrun, “Principles of Robot Motion - Theory, Algorithms, and Implementation”, MIT Press, 2005.

[73] S. Lavalle, “Planning Algorithms”, Cambridge University Press, 2006

[74] G. Chirikjian, “Theory and Applications of Hyper-Redundant Robotic Manipulators”, 1992.

[75] G. Chirikjian and J. Burdick, “An obstacle avoidance algorithm for hyper-redundant manipulators”, Cincinnatti, OH, 1990.

[76] G. Chirikjian and J. Burdick, “Design and experiments with a 30 DOF robot”, Atlanta, GA, 1993.

[77] G. Chirikjian, “Hyper-Redundant Robot Mechanisms and Their Applications”, Osaka, Japan, 1991.

[78] L. Pfotzer, S. Klemm, A. Rönnau, J. M. Zöllner, and R. Dillmann, “Autonomous navigation for reconfigurable snake-like robots in challenging, unknown environments,” *Robotics and Autonomous Systems*, vol. 89, pp. 123-135, 2017.

[79] M. S. Menon, V. C. Ravi, and A. Ghosal, “Trajectory Planning and Obstacle Avoidance for Hyper-Redundant Serial Robots,” *ASME. J. Mechanisms Robotics*, vol. 9, 2017.

[80] E. K. Xidias, “Time-optimal trajectory planning for hyper-redundant manipulators in 3D workspaces,” *Robotics and Computer-Integrated Manufacturing*, vol. 50, pp. 286-298, 2018.

[81] J. Zhao, L. Zhao, and Y. Wang, “A Novel Method for the Motion Planning of Hyper-redundant Manipulators Based on Monte Carlo,” *Mechanism and Machine Science*, vol. 408, pp. 11-22, 2017.

[82] A. Motahari, H. Zohoor, and M. H. Korayem, “A new motion planning method for discretely actuated hyper-redundant manipulators,” *Robotica*, vol. 35, no. 1, pp. 101–118, 2017.

[83] M. D. Graca and J. T. Machado, “An evolutionary approach for the motion planning of redundant and hyper-redundant manipulators”, *Nonlinear Dynamics*, pp. 115-129, 2010.

[84] A. Shukla, E. Singla, P. Wahi and B. Dasgupta, “A direct variational method for planning monotonically optimal paths for redundant manipulators in constrained workspaces”, *Robotics and Autonomous Systems*, pp. 209-220, 2013.

[85] N. Shvalb, B. B. Moshe and O. Medina, “A real-time motion planning algorithm for a hyper-redundant set of mechanisms”, *Robotica*, pp. 1327-1335, 2013.

[86] D. Trivedi, C. Rahn, W. Kier and I. Walker, “Soft robotics: Biological inspiration, state of the art, and future research,” *Applied Bionics and Biomechanics*, vol. 5, no. 3, pp. 99-117, 2008.

[87] I. Walker, “Continuous Backbone 'Continuum' Robot Manipulators”, *ISRN Robotics*, vol. 2013, 2013.

[88] R. L Norton, "Machine design, an integrated approach", (Pearson, Edition 5), 2013.

תקציר

בפרויקט זה אנחנו מציגים רובוט סריאלי שנע באמצעות מספר מינימלי של מנועים (MASR – Minimally Actuated Serial Robot). רובוט זה מורכב מזרוע אשר מכילה 10 חוליות ומפרקים סיבוביים פאסיביים, ומערכת הנעה ניידת שנעה לאורך הזרוע על מנת להגיע למפרקים הרצויים ולסובב אותם. לאחר שמערכת ההנעה עוזבת את המפרק לבא אחריו, המפרק נשאר נעול באמצעות שימוש בתמסורת חלזונית. השאת חפצים לאורכה של הזרוע מתאפשרת באמצעות צבת אשר מחוברת למערכת ההנעה הניידת. השימוש במערכת ניידת לצורך העברת החפצים מציג מכניזם חדשני ומאפשר הפחתה בזמן הנדרש לביצוע המשימה. באמצעות שימוש במנוע צעד לינארי ניתן לשלוט בתנועה האנכית של המכניזם במרחב התלת ממדי.

לאורך העבודה אנחנו מציגים את התכן המכאני של הרובוט אשר מורכב מ-10 חוליות ומפרקים, ומציגים את מערכת הבקרה שתוכננה לצורך הנעת המכניזם באופן אוטומטי. בהמשך, אנחנו מציגים אלגוריתם לתכנון התנועה של הרובוט אשר נועד להפחית את זמן העבודה הדרוש לביצוע משימה ואת המרחק אותו נדרשת מערכת ההנעה הניידת לעבור. מספר ניסויים אשר בוצעו באמצעות האבטיפוס שפיתחנו ממחישים את היתרונות הרבים של רובוט MASR: המשקל הנמוך שלו בהשוואה לרובוטים סריאליים דומים, היכולת שלו לעבור התאמות ושינויים בקלות בהתאם למשימה הנדרשת הודות לעובדה כי הזרוע נטולת חווטים לכל אורכה, כפי שניתן לראות בסרטונים המצורפים.

מילות מפתח: רובוט סריאלי, הנעה מינימלית, אקטואטור נייד, תכן מכאני.

שבט ה׳תש״פ   יולי 2020

אוניברסיטת בן גוריון בנגב

הפקולטה למדעי ההנדסה

המחלקה להנדסת מכונות

תנכון ומידול של רובוט טורי מינימליסטי

חיבור זה מהווה חלק מהדרישות לקבלת תואר מגיסטר בהנדסה

מאת: יותם אילון

מנחה: ד״ר דוד זרוק

מחבר: יותם אילון תאריך: **19.07.2020**

מנחה: דוד זרוק תאריך: **19.07.2020**

אישור יו״ר ועדת תואר שני מחלקתית: ד״ר בני בר-און יו״ר לימודי מוסמכים המחלקה להנדסת מכונות תאריך: 21.7.20

שבט ה׳תש״פ יולי 2020

אוניברסיטת בן גוריון בנגב

הפקולטה למדעי ההנדסה

המחלקה להנדסת מכונות

תכנון ומידול של רובוט טורי מינימליסטי

חיבור זה מהווה חלק מהדרישות לקבלת תואר מגיסטר בהנדסה

מאת: יותם אילון

שבט ה׳תש״פ   יולי 2020